A high-resolution modeling study of the Western Iberian Margin mean and seasonal upper ocean circulation

Rita Nolasco, Ana Cordeiro Pires, Nuno Cordeiro, Bernard Le Cann & Jesus Dubert

Ocean Dynamics
Theoretical, Computational and Observational Oceanography

ISSN 1616-7341

Ocean Dynamics
DOI 10.1007/s10236-013-0647-8

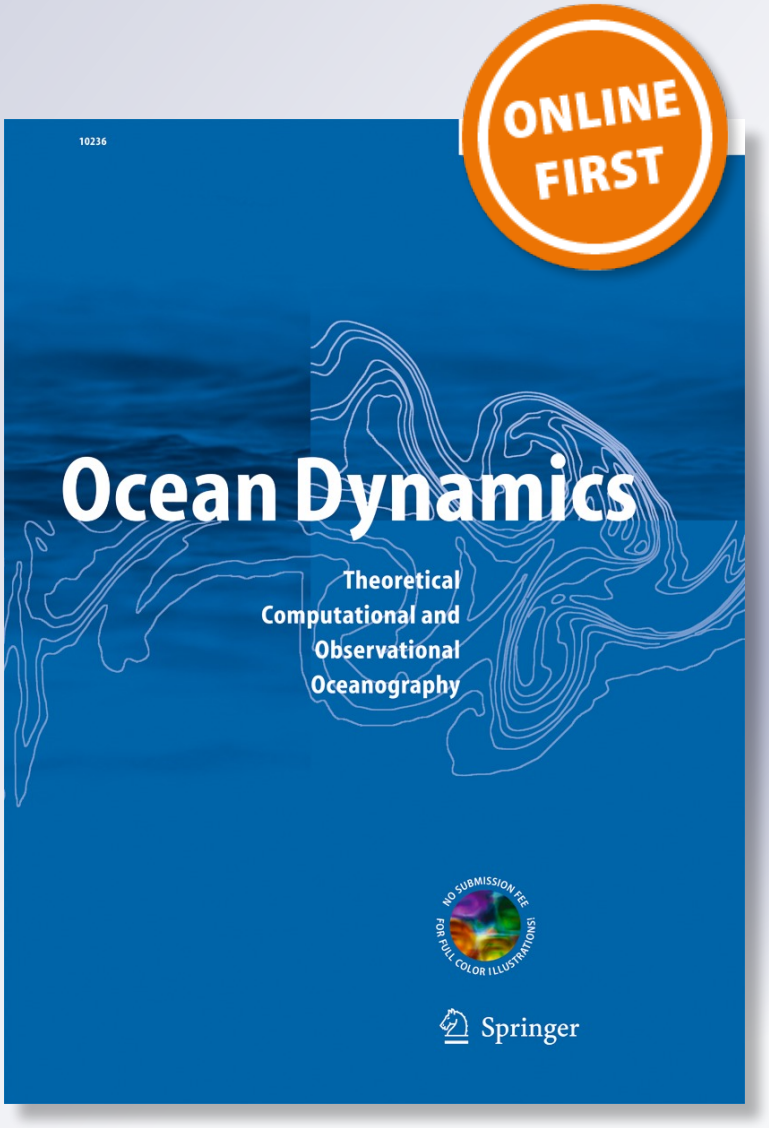

Springer

Ocean Dynamics
DOI 10.1007/s10236-013-0647-8

A high-resolution modeling study of the Western Iberian Margin mean and seasonal upper ocean circulation

Rita Nolasco · Ana Cordeiro Pires · Nuno Cordeiro · Bernard Le Cann · Jesus Dubert

Received: 14 November 2012 / Accepted: 13 August 2013

Abstract The mean seasonal hydrography and circulation of the Western Iberian Margin (WIM) are studied by means of a high-resolution configuration of the Regional Oceanic Modeling System. A comparison of 5-year model averages for January and July with climatological datasets shows a general good agreement in the reproduction of the mean water mass properties and hydrographic distribution. We find that there is a prevailing tendency for slope poleward flow at about 80–100 km offshore at all latitudes from the surface to 1,500 m with strong vertical coupling. This northward flow, which is mainly along slope and amounts up to 8–10 cm s^{-1}, exhibits several mean flow recirculation regions on its way and evidences of an offshore pathway of poleward flow. Transports at different zonal sections further confirm the poleward flow tendency with two peaks of poleward transport in summer (3–10 Sv) and winter (2–7 Sv). The transport time series emphasize the seasonal character of the alongshore circulation and the interannual intrinsic variability of the circulation, since the forcing fields are climatological. As a conceptual essay with the purpose of assessing the Mediterranean Water flow influence on the WIM mean circulation, a second model configuration is setup, where the Mediterranean outflow into the study domain is removed. We find that there is an attenuation of the mesoscale field, but the slope poleward flow intensifies and remains as a mean dynamical feature closer to the upper slope.

Responsible Editor: Matthew Robert Palmer

R. Nolasco (✉) · A. C. Pires · N. Cordeiro · J. Dubert
Department of Physics, Campus de Santiago, Centro de Estudos do Ambiente e do Mar (CESAM), University of Aveiro, 3810-193 Aveiro, Portugal
e-mail: rita.nolasco@ua.pt

B. Le Cann
Laboratoire de Physique des Océans, UMR 6523 CNRS/UBO/IFREMER/IRD, Université de Bretagne Occidentale, Brest, France

Keywords Western Iberian Margin · Numerical modeling · Poleward flow · Upwelling systems

1 Introduction

The Western Iberian Margin (WIM; see Fig. 1, domain SD) is located between two offshore large-scale oceanic systems: to the north, the North Atlantic Current flowing in the NE direction; to the south, the Azores Current flowing eastward with complex interactions with the Gulf of Cadiz. This region is characterized by a weak large-scale circulation, mostly southward, with typical velocities of a few centimeters per second, and frequently named the Portugal Current (Saunders 1982).

At the coastal transition zone, the circulation along the WIM is largely influenced by the presence of the atmospheric anticyclonic system named Azores High, whose position oscillates between northern locations off the Iberian Peninsula during summer and a southern position during winter in front of Morocco, while the Iceland low intensifies leaving room for the eastward passage of low pressure systems that introduce a strong variability in the circulation along the WIM during wintertime.

These atmospheric regimes are the reason why in late spring and summer, there is coastal upwelling, that is, deep, cool, nutrient-rich waters upwell and are advected equatorward, resulting in an offshore displacement of surface warm waters and phytoplankton blooms (see review by Relvas et al. 2007). The thermohaline structure of the water masses, consisting in large-scale temperature and salinity meridional gradients (Peliz et al. 2003), together with wind forcing, generate a system of poleward currents along the Atlantic Iberian Peninsula observed mainly during autumn and winter, as described in the classic references of Frouin et al. (1990) and Haynes and Barton (1990) for the western Iberian

Published online: 13 September 2013

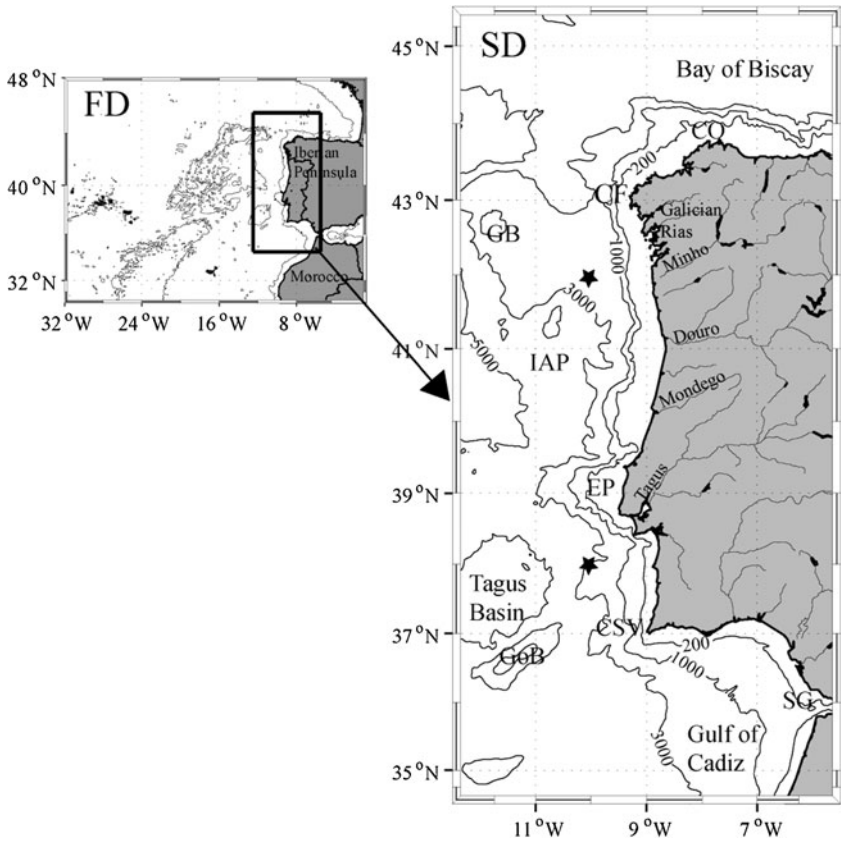

Fig. 1 Map of the region under study: the first domain (*FD*), comprising the Iberian Peninsula, the north of Africa (Morocco) and the Azores Islands; the local domain (*SD*) marked with the main bathymetric and topographic features: Strait of Gibraltar (*SG*), Cape St Vincent (*CSV*), Gorringe Bank (*GoB*), Estremadura Promontory (*EP*), Iberian Abyssal Plain (*IAP*), Galicia Bank (*GB*), Cape Finisterre (*CF*), and Cape Ortegal (*CO*). The *stars* mark the locations of analysis for Section 3.2.2

Peninsula and continuing along the Bay of Biscay as described by Pingree and Le Cann (1990). This northward circulation is typical of midlatitude eastern continental margins (Neshyba 1986). A consensual denomination for this flow is the Iberian Poleward Current (IPC). The classic view of the IPC presents it as an upper slope baroclinic current, associated with the downwelling of the isopycnal field in a width of about 40 km and positive temperature and salinity anomalies from the surface down to typically 400 m. It was suggested that poleward flows are not a winter phenomenon only but are present throughout the year (see reviews by Peliz et al. 2005 and Relvas et al. 2007).

Below the surface waters, the Mediterranean Water (MW) is of central importance for the circulation in the region. The MW enters the domain through the Strait of Gibraltar and flows at depth along the Gulf of Cadiz and the WIM slope. The resulting intermediate-level current is called Mediterranean Undercurrent (MU) in the Gulf of Cadiz (Ambar and Howe 1979) and Mediterranean Water Vein along the WIM (Daniault et al. 1994); it should be noted that the Mediterranean Water Vein is not the only pathway by which MW reaches the Atlantic. Upon exiting the 300 m deep Strait of Gibraltar, the dense MW flows downslope within the Gulf of Cadiz until it reaches neutral buoyancy; afterwards, along the WIM, it flows at mid-depths often in two cores, typically at 800 m (the upper core), where a temperature maximum is reached, and at 1,200 m (the lower core), the depth at which the salinity maximum is found. The signature of the hydrographic properties of both cores decreases (notably the upper core) in the poleward direction along the WIM. Associated with this flow, there are mesoscale structures that are formed and which are responsible for a relevant part of this water mass properties transport: the Mediterranean eddies (Meddies), anticyclonic vortices with radii of several tens of kilometers, centered around 700 and 1,300 m deep (Bower et al. 1995). Meddies propagate typically southwestwards into the North Atlantic (Richardson et al. 2000).

The numerical study of the circulation of the WIM is a challenge for modelers for several reasons: (1) the presence of a narrow shelf and a steep slope (up to 10 %), as well as the presence of numerous canyons and promontories, requiring high resolution to properly resolve the shelf/slope circulation in presence of realistic stratification; (2) the presence of a unique oceanographic feature, which is the MU, generated at the Strait of Gibraltar and spreading into the NE Atlantic giving rise to the large-scale Mediterranean Water (MW) anomaly; (3) the influence of the open ocean circulation (the Azores Current system and meridional pressure gradients) on the coastal transition zone, that forces the circulation in this region.

In this way, there is a need for high-resolution studies that may deal with the factors mentioned above, with special

attention to the different scales that influence the circulation of the WIM, ranging from the few kilometers of the Strait of Gibraltar dynamics, to the hundreds to thousands kilometers scale of the Azores Current system. These features compelled us to perform a multiscale simulation based on nesting techniques, as detailed below.

In what concerns numerical modeling regional studies at the full scale of the region, some previous works contributed to the study of this particular circulation. Some of them were carried out at a low resolution of about 9 km (Stevens et al. 2000; Coelho et al. 2002) and focused on spring and winter circulation; others were idealized studies at a high resolution (Røed and Shi 1999; Peliz et al. 2003). Batteen et al. (2000, 2007) carried out sensitivity studies in order to assess the different mechanisms controlling the circulation in the region. The study by Serra et al. (2010) resolves the circulation in this region with realistic forcing and high resolution, focusing on the study of the influence of the MW vein on the surface circulation, with emphasis on the mesoscale phenomena. On the other hand, from the point of view of operational oceanography of the Western Iberian Margin, Mateus et al. (2012) focused on the application of an operational configuration (~1/16° resolution) to discuss its potential for products and services for scientific and coastal management activities.

In the neighborhood of the region and also at a high resolution, Friocourt et al. (2007) and Peliz et al. (2007) studied the Bay of Biscay and the Gulf of Cadiz circulation, respectively.

Although the three major distinctive phenomena of the WIM referred to above—upwelling, poleward flow, and Mediterranean outflow—have an independent dynamical origin, they are intimately linked and should be studied in an integrated manner. This is the main challenge for the present work.

The present configuration includes the WIM region, the Western Bay of Biscay, and the Gulf of Cadiz. It is intended to study the equilibrium hydrography and circulation in the surface layers, the underlying Central Waters, and the intermediate Mediterranean Waters.

In order to do that, numerical simulations for the WIM region forced by climatological heat and momentum fluxes were setup. In the present work, we intend to discuss the mean circulation that arises from the intrinsic variability of the model in the absence of any external interannual atmospheric or oceanic forcing.

Using climatological forcings, the model results achieve a realistic circulation, reflected by a mesoscale field (not discussed in this work), and a mean field, which is described and discussed in the light of the observations. The results discussed in this work intend to contribute to the understanding of the IPC, not only during winter as is classically studied, but also in the summertime, when the dominant poleward flow on the outer slope coexists with equatorward flow, in agreement with the observations. It is also intended to discuss the generation of vorticity structures of the mean flow along the WIM and its relation to the topography and the large-scale circulation. The links between the surface and the intermediate circulation are also discussed as is the resulting circulation in the hypothetical case of suppression of the MW overflow.

The outline of this work is as follows: in Section 2, we describe the methodology and the ocean model configurations set up for this study; in Section 3, we present a comparison of model results with observational data and we characterize the mean annual and seasonal hydrography and circulation of the WIM region; in Section 4, we study the influence of the MW in the WIM circulation; and in Section 5, we discuss the results.

2 Methods and data

2.1 Ocean model

A high-resolution nested configuration of the Regional Ocean Modeling System (ROMS; Shchepetkin and McWilliams 2003) is used to simulate the seasonal dynamics of the Iberian System. ROMS is a split-explicit, free-surface, topography-following-coordinate model designed to resolve regional problems (Shchepetkin and McWilliams 2005). ROMS solves the incompressible primitive equations based on the Boussinesq and hydrostatic approximations and is coupled with advection/diffusion schemes for potential temperature and salinity as well as a nonlinear equation of state. The advection scheme is based on the work done by Marchesiello et al. (2009) in order to reduce spurious diapycnal mixing in sigma coordinate models characteristic of higher-order diffusive advection schemes. This scheme involves the split of advection and diffusion as a biharmonic operator. Vertical mixing consists in the K-profile parameterization scheme (Large et al. 1994).

2.1.1 Model configuration

(a) Large domain

The strategy to manage a large range of scales consists in the implementation of a two-domain approach as shown in Fig. 1. A large-scale first domain (FD) is run independently in order to provide initial and boundary conditions to our second domain (denoted SD hereafter) through an offline nesting. The first domain horizontal resolution is 1/10° (~9.5 km in longitude) and the main aim for this domain is to resolve the large-scale circulation features such as the Azores Current and their interaction with the Atlantic margin of the Iberian Peninsula.

For this domain, 30 sigma vertical levels are used with a stretching factor of θ_s=7 and θ_b=0 to conserve a good

near-surface resolution over the entire domain. The bathymetry is based on ETOPO1 (Amante and Eakins 2009) with corrections near the slope and a smoothing filter to fulfill the $r=\Delta h/2h$ criterion (Haidvogel and Beckmann 1999), $r<0.2$.

The World Ocean Atlas 2009 (WOA-2009) climatology is used as the initial value for the temperature (Locarnini et al. 2010) and salinity (Antonov et al. 2010) fields and also to recycle these fields along the nudging bands, providing open boundary conditions. Surface fluxes are obtained from the Comprehensive Ocean–Atmosphere Dataset (COADS; da Silva et al. 1994) interpolated to the grid with the Roms_tools (Penven et al. 2008) package. This climatology derived from the National Oceanic and Atmospheric Administration (NOAA) global data retrieval program (http://icoads.noaa.gov) and consists in one value per month for each parameter, computed for the time period 1945–1989. That is, COADS has no interannual variability, only seasonal. Its spatial resolution is of 0.5° for all parameters except for sea surface salinity, for which it is of 1°. Initial velocities are zero and monthly geostrophic velocities (with level of reference, 1,200 m) and Ekman velocities are computed from the climatology and applied along the open boundaries.

The Mediterranean water is introduced by nudging, applied to the Gulf of Cadiz and Western Iberia as described in Peliz et al. (2007), in order to restore the hydrographic properties (T and S) of the Mediterranean levels, so as to generate realistic Mediterranean water hydrographic properties.

The open boundary conditions were based on Marchesiello et al. (2001). These conditions are suitable for long-time integration and are characterized by inflow (outflow) nudging timescales of 1 (360)day for tracers and 10 (360)days for momentum, respectively. Sponge layers 120 km wide were applied along the edges, with a lateral viscosity coefficient ranging from 600 m^2/s at the boundary to zero in the interior. Explicit viscosity and diffusivity is null; a linear drag formulation with coefficient $r=3\times10^{-4}$ m s^{-1} is applied at the bottom. The objective of the large grid is to achieve a good representation of the Azores Current transport and the connection of the Azores Current with the Gulf of Cadiz where the western and southern boundary of the high-resolution grid is located.

(b) High-resolution domain

The target domain, SD (second domain, see Fig. 1), has a horizontal resolution of 1/27° (~3 km in longitude) and includes the Gulf of Cadiz, the WIM, and part of the western Bay of Biscay, extending for ~1,300 km in the meridional direction from 34 to 46°N. In the zonal direction, the domain extends from the Strait of Gibraltar, located at 5.5–12.5°W, representing a width of about ~600 km.

Sixty sigma vertical levels with $\theta_s=4$ and $\theta_b=0$ are used to properly resolve the Mediterranean undercurrent with enough near-bottom resolution. In this way, the grid has 60×188×389 cells. The topography by Sibuet et al. (2004) was used; it has a resolution of ~1 km and was smoothed in order to fulfill the same r factor criterion (r factor less than 0.2) of the large-scale domain.

The forcing for this high-resolution configuration domain is the same as the one used for the large-scale FD domain. The initialization and the boundary conditions are obtained using year 5 from FD with average data stored every 3 days. To test the sensitivity of the model results to this choice, an additional experiment to the main simulation, was run using year 7 of FD simulation, instead of the year 5, showing results similar to the main run ones described below.

Also, like for the large-scale simulation, a nudging sponge layer is introduced. Concerning the boundary conditions of the SD domain, radiation conditions of Marchesiello et al. (2001) are also used. The nudging coefficients at the edges are the same as the ones used for FD configuration. However, the sponge layers at the edges are applied to a band of 40 km with a lateral viscosity coefficient ranging from 200 m^2/s at the boundary to zero at the interior of the domain. A quadratic drag coefficient of 5×10^{-3} is used for the bottom friction parameterization. At the Strait of Gibraltar, at the southeastern boundary, the water exchange with the Mediterranean basin is explicitly represented in the domain, through a fixed boundary (as in Peliz et al. 2007): it consists in the imposition of vertical profiles of temperature, salinity, and zonal velocity at the boundary located at the Strait. This condition is designed to setup a two-layer system consisting in a transport of 0.8 Sv of Atlantic water leaving the domain through the surface layer and 0.7 Sv of Mediterranean water entering the domain through the lower layer. No attempt to introduce seasonality or interannual variability in these fluxes was done. The process of entrainment of Atlantic Central Waters with the MU is also parameterized by increasing the viscosity and diffusivity coefficients in a region in which the MW is strongly mixed with the overlying Atlantic waters, until the MW vein forms along the northern slope of the Gulf of Cadiz.

The inflow of freshwater in the ocean, originating from the main rivers of the region (the most important rivers are identified in Fig. 1), is included. For the Portuguese rivers, climatological values were provided by INAG (Water Institute of Portugal); the information on the Spanish rivers was given by Barja and Lestegás (1992).

The spin-up time for this domain, during which the kinetic energy stabilizes, is 5 years, as the adjustment time of the MU along the western and northern Iberian Margin is quite a slow process. Thus, the model is run for 14 years and the analysis presented here is done for years 10–14 in order to show the seasonal and interannual variability during that period.

(c) Solution without Mediterranean Water

A sensitivity experiment is performed in order to study the resulting circulation without the MW spreading through the Strait of Gibraltar. For that, the large-scale domain FD is run for 15 years with initial conditions from the World Ocean Atlas 2009. The condition to maintain MW outflow was relaxed by turning off the nudging condition applied at the Gulf of Cadiz until the effect of the MW salinity and temperature anomalies disappears as much as possible by diffusion. Boundary conditions for SD are built from the results of this FD configuration with a closed boundary condition at the Strait of Gibraltar. SD is then run following the same methodology described in the previous section for 14 years.

2.2 Climatology and satellite products

In the following section, model output is compared to climatological data. Two datasets were chosen to carry out this comparison: the recent climatological GHER atlas for the Northeast Atlantic (Troupin et al. 2010; hereafter, GHER-NEA climatology) and satellite products. The GHER-NEA climatology was chosen for its high resolution (0.1°), which properly resolves the slope and shelf regions unlike most available climatologies, and both temperature and salinity are compared to model results. For the sea surface temperature (SST), the comparison is carried out with data from the advanced very high resolution radiometer of the NOAA. The data was extracted from the EUMETSAT Ocean & Sea Ice Satellite Application Facility (www.osi-saf.org) and was made available by CERSAT (IFREMER, France). The product has an approximate resolution of 2 km. The final data consists in 7-year averages, corresponding to years 2002–2008, for January and July, of the night satellite sweep (hereafter satellite climatology).

3 Results

The first part of this section is dedicated to introducing the main features of the hydrography of the region, assessing the reliability of the model in resolving the hydrography of WIM and its seasonal variability and comparing model output for SD with the climatological data. This comparison is carried out by means of surface horizontal field maps, θ–S diagrams for water mass characterization, and vertical sections of hydrographic fields along different latitudes. The second part of this section focuses on studying the mean seasonal circulation of the region and the vertical structure of the flow from model output through velocity fields and the analysis of meridional transport. A second solution without MW as described above is also analyzed at the end of the section.

3.1 First domain model configuration

The FD domain was designed to solve the large-scale circulation in order to provide boundary conditions to the target domain SD. It is not intended to discuss the resulting circulation from this domain but to show an example of how the large-scale circulation is solved for this domain. For that purpose, a eddy kinetic energy (EKE) comparison between altimetry and FD output is done in Fig. 2. Altimetry weekly data was obtained from Archiving, Validation, and Interpretation of Satellite Oceanographic (AVISO) for the period October 1992 to July 2011. The signature of the Azores Current is clear between 33 and 36°N and the signal extend eastwards to

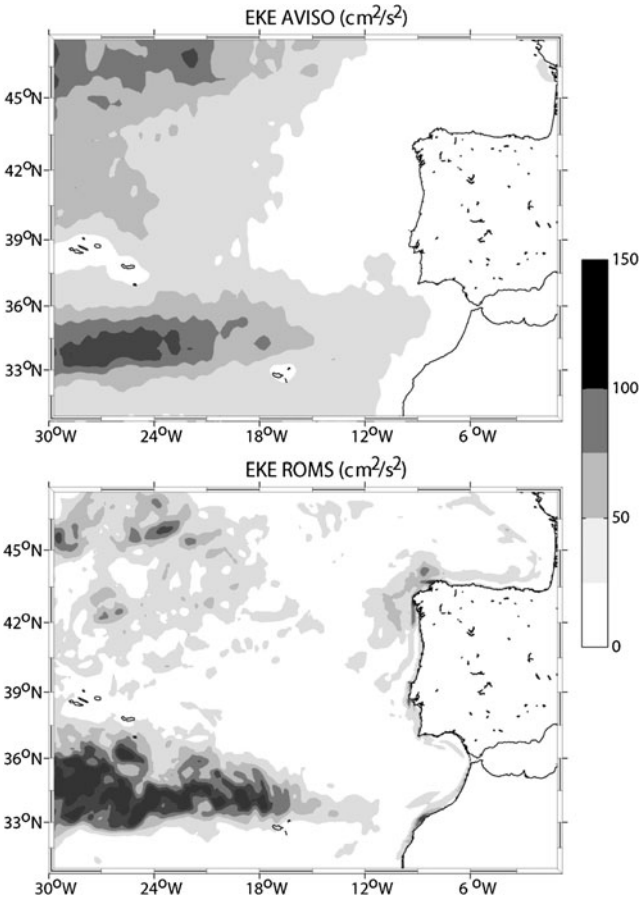

Fig. 2 A EKE comparison between altimetry (from AVISO) (*top*) and FD output (*bottom*)

~12°W in both. There is also evidence of the North Atlantic Current at the northwestern corner of the FD domain. In terms of magnitude, EKE is more intense in ROMS for the Azores Current and more intense in AVISO for the North Atlantic Current. Nevertheless, we find that the comparison is acceptable and we conclude that FD is reproducing correctly the regional dynamics. Other diagnostics (not shown) were done in order to check that the large-scale hydrography and circulation of FD domain are suitable for use as boundary conditions for the target domain, SD.

3.2 Hydrography and comparison to climatological data

3.2.1 Surface fields

Figure 3 (4) presents January (July) mean SST (upper row) and salinity (SSS, lower row) of both SD and climatology as well as the difference field between the modeled and the climatological fields.

(a) Winter

During winter (Fig. 3), both SD and climatologies show the existence of a meridional gradient of sea surface temperature and salinity. Moreover, a tongue of saltier and warmer water centered at approximately 9.5–10°W is associated with the poleward advection of waters of subtropical origin, frequently referred to in the literature as the IPC (Álvarez-Salgado et al. 2003). Although this tongue is visible in both SST and SSS, it is less evident in the SST satellite field. Furthermore, the poleward penetration of the climatological tongue reaches farther north than the SD one, causing a difference of about −0.1 in salinity between 39 and 42°N.

Along the continental shelf region, north of the Estremadura Promontory (39°N), we observe the presence of a band of buoyant fresher and colder waters in the SST and SSS climatologies, as well as in the SD averages. This band is associated with the presence of winter river inflow along the western coast mainly contributed to by Tagus, Mondego, Douro, Minho, and the Galician Rias rivers (see Fig. 1). This freshwater signature remains trapped on the continental shelf generating the Western Iberian Buoyant Plume (WIBP; Peliz et al. 2002; Otero et al. 2008).

(b) Summer

During summer (Fig. 4), the most important phenomenon observed is coastal upwelling induced by the

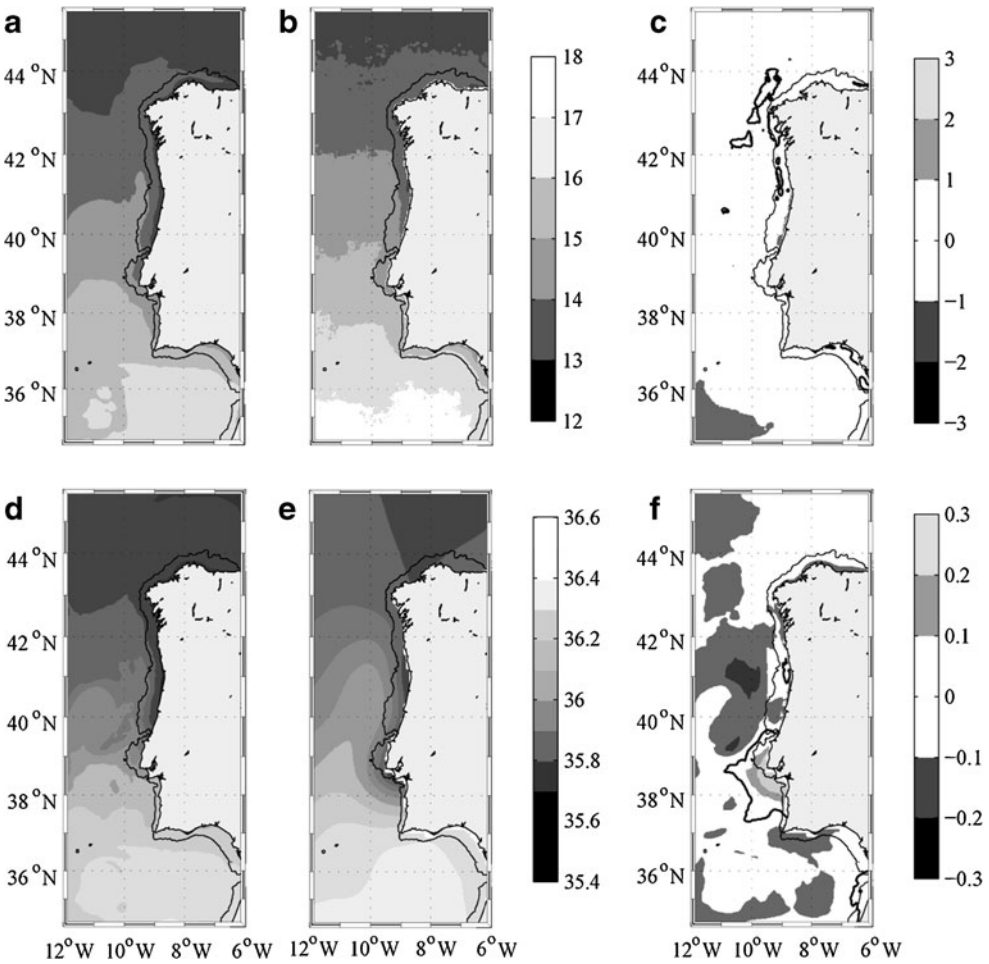

Fig. 3 Sea surface temperature (SST) in degree Celsius (**a**–**c**) and sea surface salinity (SSS) (**d**–**f**) for January. **a**,**d** The 5-year mean of ROMS output; **b**,**e** 7-year mean of advanced very high resolution radiometer at 02 h and GHER-NEA climatology, respectively; **c**,**f** difference between **a** and **b** and between **d** and **e**, respectively. *Thick contours* outline null difference. The 200 m isobath is shown in *thin black contour*

predominant equatorward winds along the WIM, which result in the presence of a coastal band of cold and fresh waters.

The main patterns of the July average temperature and salinity for the offshore region are well reproduced in SD resulting in small temperature and salinity differences (Fig. 4c,f). However, SD tends to overestimate the intensity of the upwelling phenomenon and therefore exhibits a coastal water band that is colder than the satellite climatology. As discussed by Veitch et al. (2010), and references herein, the climatological winds do not account for the drop-off of the wind stress in the neighborhood of the coast.

There are also regions in which SD, on the contrary, overestimates the surface temperature. Along the Galician coast, north of Cape Finisterre, unlike SD results, filaments like the Finisterre filament (43°N), are frequently observed by satellite in this area (Torres et al. 2003).

Other regions where SD temperatures are warmer than observed are the northern Gulf of Cadiz (Portuguese southern coast) and the northern coast of Morocco. These regions are influenced by gap winds that consist in strong easterly winds associated to pressure differences between both sides of the strait of Gibraltar (Peliz et al. 2009) not represented in the climatological winds.

The summer SSS field (Fig. 4d) is characterized by the upwelling of Eastern North Atlantic Central Waters of northern origin ($ENACW_{sp}$, see Section 3.2.2 for details), which is advected southward. This upwelled water has a typical salinity of about 35.8. Overlying the upwelled Central Water, there is a low salinity surface water (lower than 35.7) observed in the GHER-NEA climatology (Fig. 4e), which is associated with the remnant of the WIBP advected offshore by Ekman transport, giving rise to a low salinity plume at the surface.

3.2.2 Water masses

The main water masses of the upper layers observed in the region of study along the WIM originate from the subpolar or the subtropical branches of the Eastern North Atlantic Central Waters, $ENACW_{sp}$ and $ENACW_{st}$, respectively, as defined by Ríos et al. (1992). Below the Central Waters lies the MW that

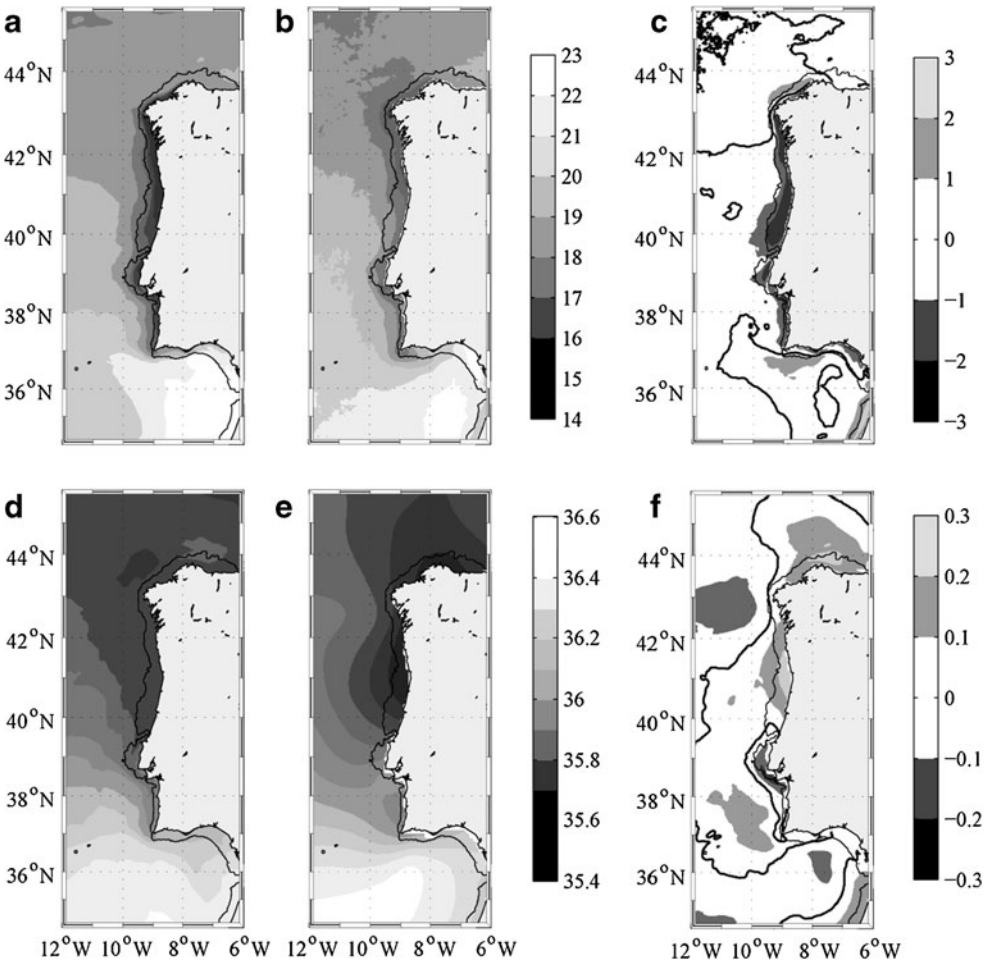

Fig. 4 Same as Fig. 3 but for July

flows through the Gulf of Cadiz and the entire basin with a typical tongue structure, reaching the Bay of Biscay as described in the literature and as observed in the available climatologies (WOA-2009; Reynaud et al. 1998; Iorga and Lozier 1999; Troupin et al. 2010). Below 1,500 m, there is the signature of the Labrador Sea Water described by Paillet et al. (1998). Although its hydrographic properties are reasonably well-represented in SD (not shown), this water mass, as well as the deeper layer North Atlantic Deep Water, is not discussed in this work.

To compare the SD water mass properties to the climatological values, θ–S diagrams were elaborated for two boxes (1° latitude×1° longitude) centered at 10°W and 38 and 42°N (see Fig. 1 for location). These diagrams are displayed in Fig. 5. For each box, monthly (January, April, July, and October) mean profiles of potential temperature and salinity were calculated for years 10–14 of the simulation (one dashed line per year in order to show the interannual variability) and are superimposed to the GHER-NEA climatology (solid line).

The seasonal evolution of the thermohaline properties of the Central and surface waters is reproduced by SD when compared to the climatological values. As for the Central Water properties of both SD and climatology, by comparison with the standard straight lines in the θ–S space for $ENACW_{st}$ and $ENACW_{sp}$, it is clear that the northern (southern) region is more influenced by the presence of the subpolar (subtropical) branch of the ENACW.

For the southern region, in January (Fig. 5a), the Central Waters have their thermohaline properties superimposed with the $ENACW_{st}$ line, typical of the waters that give origin to the IPC. Below the surface, salinity decreases linearly to a minimum of 35.7 and increases downwards because of the influence of the underlying MW mass. In April (Fig. 5b), a decrease of the surface salinity maximum is observed associated with the start of the upwelling season. During summer (Fig. 5c), the seasonal heating modifies the θ–S structure at the surface, increasing the temperature of the surface layer. Furthermore, interannual variability of the temperature in the surface layers is observed. The MW mass is reproduced in SD, ranging from 36.2 to 36.35, which includes the climatological value. In October (Fig. 5d), after the upwelling season, the signature of saltier surface waters associated to the IPC is visible both in the SD and the climatology, although SD underestimates the surface salinity by about −0.1 units.

Regarding the northern region (centered at 42°N, 10°W; Fig. 5e–h), the seasonal evolution of the θ–S field follows a pattern similar to the one described for the southern region; the main differences being observed in the salinity field at the surface levels, with lower maximum values of salinity both in winter and in summer. At the MW levels, the salinity signature decreases in the poleward direction as expected.

Overall, the SD configuration not only follows the seasonal cycle of temperature and salinity for the surface and central waters, but also reproduces the MW hydrographic properties, although some negative biases are observed (as well as in the MW core depths, as discussed later).

3.2.3 Vertical structure

As a complementary analysis of the water masses in the two regions discussed above, we now study the vertical distribution of the hydrographic properties and compare the modeled values with the GHER-NEA climatology. The aim is to show and discuss the modeled temperature and salinity fields and to compare them to climatological values across two latitudes, 42 and 38°N, representative of the northern and southern WIM, respectively. The averages for SD were computed for January and July of simulation years 10–14, down to 1,500 m in depth.

(a) Winter hydrography

At 42°N (Fig. 6a,c), the winter distribution of temperature and salinity shows a general downward sloping of the isolines in the upper slope region (down to about 400 m), between 9.5 and 11°W. This downward tendency is associated with the presence of the IPC during wintertime, with salinities higher than 35.9 and temperatures around 14.5 °C (Fig. 6c). The SD IPC (Fig. 6a) shows evidence of this poleward advection at the surface; however, there is a bias of about −1 °C in temperature and about −0.1 in salinity. On the other hand, the salinity minimum of $ENACW_{sp}$ of 35.65 (see Fig. 5e) is reached at depths around 400 m, shallower than the climatological minimum (450 m). Below that depth lies the MW and thus the salinity field values increase accordingly to 36 near the slope at an approximate depth of 900 m, which is −0.1 fresher and 100 m shallower than the climatological value.

For the southern latitude, 38°N (Fig. 6b,d), the surface layers are characterized by the presence of saltier and warmer waters when compared to the northern section. In January, for the surface and central water range, the hydrographic properties reflect the straight line observed in the θ–S diagrams (Fig. 5a). Concerning the MW, below the ENACW, the SD temperature maximum (~12 °C) associated with the upper core of MW does not reach as far offshore as the climatological one (extending to 10.5°W whereas in SD the isotherm is close to the slope), but the depth at which they are found (800 m) is the same. On the other hand, the lower core SD MW salinity maximum, 36.2, is underestimated (−0.1 bias in S), as it is the depth at which this maximum is found (about 1,000 m in SD and 1,200 m in the climatology). Below the MW, the transition to LSW in SD is located at depths lower than the climatological value.

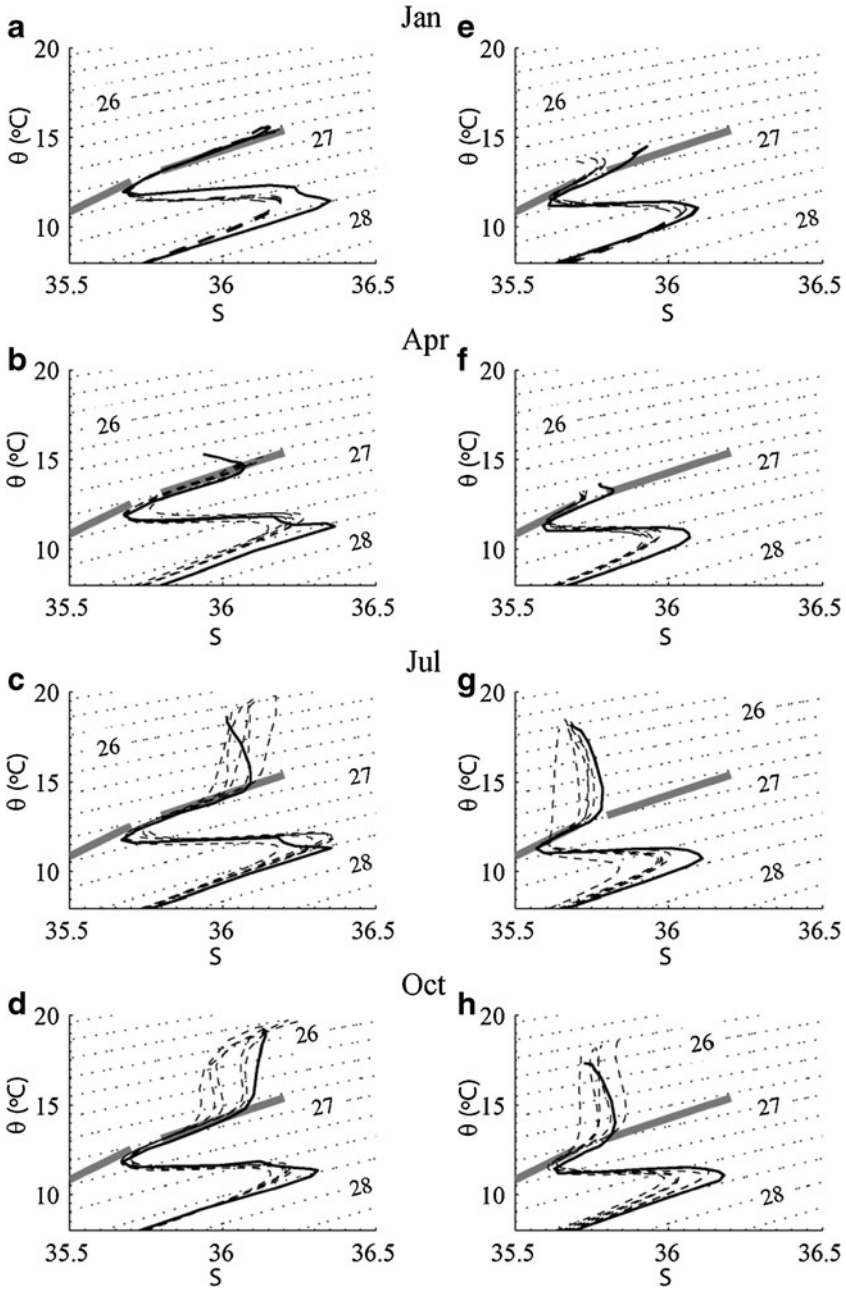

Fig. 5 θ–S diagrams monthly means of ROMS output (*dashed lines*, one per year, for years 10–14) and GHER-NEA climatology (*solid line*) for January (**a**,**e**), April (**b**,**f**), July (**c**,**g**), and October (**d**,**h**) for two regions: one centered at 38°N, 10°W (**a**–**d**), the other centered at 42°N, 10°W (**e**–**h**). Potential density anomaly (σ_θ) is superimposed in *dotted lines* every 0.2 kg m^{-3}; the *shaded line* corresponds to the standard definitions of ENACW$_{st}$ and ENACW$_{sp}$, defined as $\theta = 10+8.462\times(S-35.4)$ for the subpolar branch ($34.8<S<35.7$) and $\theta = 13.13+5.653\times(S-35.8)$ for the subtropical branch ($35.8<S<36.2$) as defined by Fiúza (1984)

(b) Summer hydrography

Like the winter situation, the summer vertical structure is analyzed for zonal sections at 42 and 38°N. At the northern section (Fig. 7a,c) the summer hydrography is well-characterized by the presence of coastal upwelling, which affects clearly the near-surface temperature field distribution on the continental shelf. The isotherms warmer than 14 °C outcrop on the shelf, generating a front in the numerical configuration. Note that the GHER-NEA climatology shows evidence of upwelling, although the frontal structure is smoothed, as expected from an observational climatological dataset.

The upwelling of the isothermal field extends down to the 13 °C isotherm at approximately 200 m in both SD and climatology. In the surface layers, summer salinity is lower than during winter because the signature of ENACW$_{st}$ is not observed (Fig. 5g) as the upwelled waters have a northern origin. A minimum of salinity is nevertheless observed, like in winter, with the 35.6 isohaline located at approximately 400 m depth.

Concerning the MW distribution in July, at 42°N, there are no significant differences with respect to wintertime in the climatology: the same salinity maximum is found at approximately 1,000 m enclosed by the 35.9

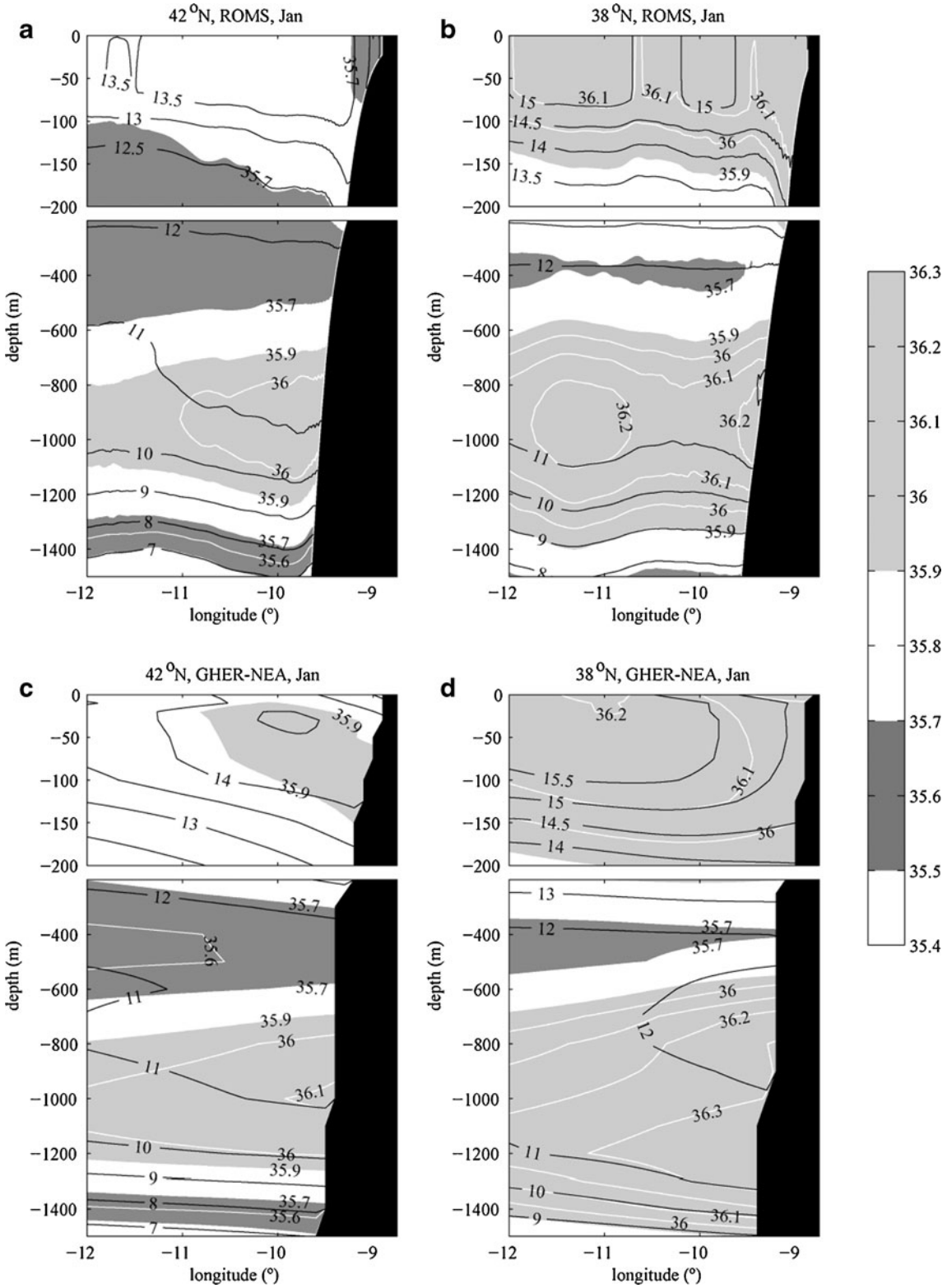

Fig. 6 Zonal sections of temperature and salinity for January: **a**,**b** 5-year means of ROMS output for 42 and 38°N, respectively; **c**,**d** GHER-NEA climatology for 42 and 38°N, respectively. Sections are down to 1,500 m and the first 200 m are enlarged. Temperature is represented in *black contours* every 0.5 °C in the upper layers and every 1 °C in the deeper layers. Salinity is depicted in *white contours* every 0.1 and *shades of gray* for specific values: MW (35.9–36.3) is represented in *light gray* and ENACW (35.5–35.7) is represented in *dark gray*. Bathymetry is colored in *black*

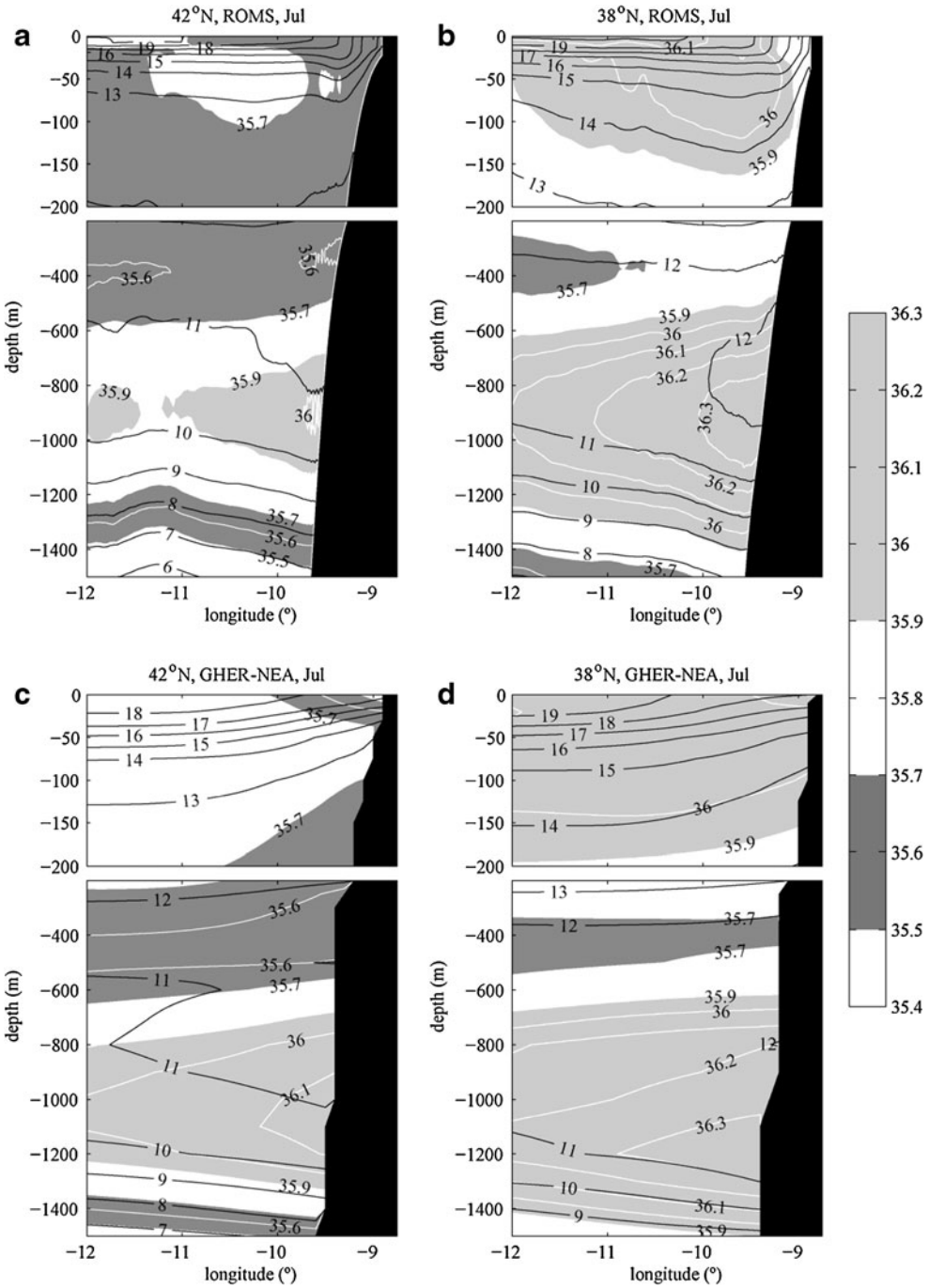

Fig. 7 Same as Fig. 6 but for July, except temperature in the upper layers is represented in *black contours* every 1 °C

isohalines between 700–800 and 1,200–1,300 m. In SD, the MW vein seems to be squeezed and the temperature field is shallower by about 100 m with respect to the winter equilibrium depth as observed by García-Lafuente et al. (2008). These authors related the shallowing of the MW vein to the mesoscale field associated with the MW vein, which may originate from the variability of the wind field.

The southern section, 38°N (Fig. 7b,d), during summer is also affected by upwelling. In this case, the outcropped isotherm is 15 °C in SD against 17.5 °C in the climatology. At the levels of the MW vein, the main difference between SD and climatology is the 200 m depth difference in the location of the salinity maximum, whereas SD reaches the same climatological maximum of 36.3.

(c) Winter vertical meridional section.

The surface layers meridional distribution of temperature and salinity fields along the WIM at 11.5°W (Fig. 8) shows evidence of a large-scale gradient with

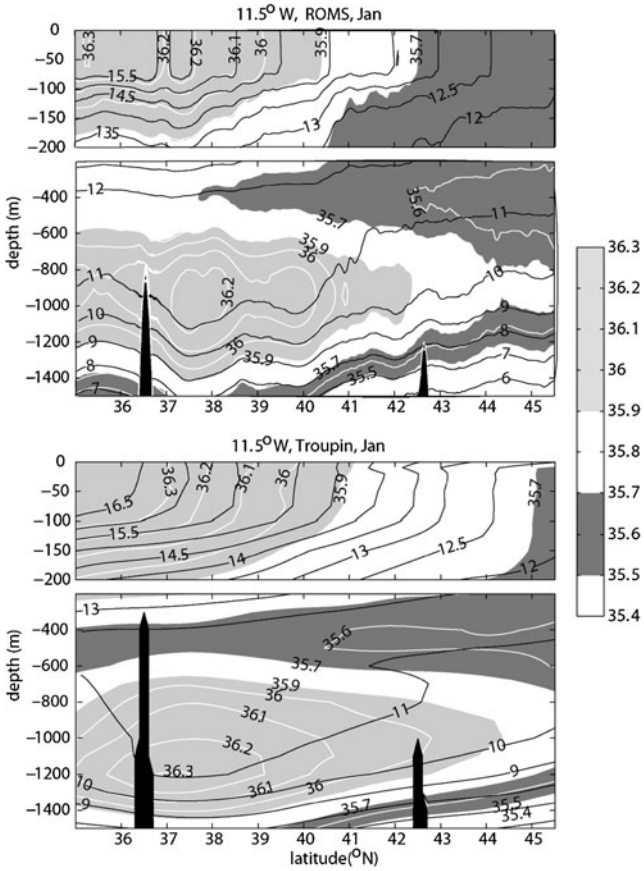

Fig. 8 Meridional section of temperature and salinity at 11.5°W for January: **a** 5-year means of ROMS output, **b** GHER-NEA climatology

southern warmer and saltier waters of subtropical origins and northern colder and fresher waters of subpolar origins. A frontal region, frequently observed between 38 and 40°N and denoted by Western Iberia Winter Front (Peliz et al. 2005) separates both regions.

This meridional density gradient is partly at the origin of the Iberian Poleward current system (Peliz et al. 2003). A proper representation of the meridional distribution of hydrographic fields is needed to obtain a realistic poleward current system along the WIM.

A comparison of ROMS monthly averages of temperature and salinity and the GHER-NEA climatological fields for January was done (Fig. 8). We observe similar meridional gradients of temperature and salinity in the upper levels (0–200 m), although ROMS presents lower salinities north of 43°N and south of 37°N (roughly differences of −0.1) and lower temperatures of about −0.5 °C to the north reaching 1 °C to the south. At depth, both the ENACW and the MW signatures are clearly observed, the former at 400–600 m with typical salinities of 35.6–35.7 and the latter centered at 1,000–1,200 m with maximum salinities of 35.2–35.3 and a temperature of 11 °C.

3.3 Mean flow structure

The main focus of this section is the analysis of the circulation in the WIM resulting from the process of adjustment of the hydrographical fields. Horizontal slices at 50 and 1,000 m depth showing monthly means for years 10–14 of the SD run of the salinity and velocity fields for January and July are displayed in Fig. 9. In addition, vertical slices of the alongshore circulation at 43°N are displayed in Fig. 10, also for January and July monthly means.

(a) Winter circulation

One of the main dynamical features at the western Gulf of Cadiz is the presence of a permanent cyclonic circulation (C1 in Fig. 9b), which is part of the structure usually referred to a topographic β-plume circulation (Kida et al. 2008). Lamas et al. (2010) provided observational evidence of the structure. This cyclonic vortex is stronger at the surface, but has a clear signature at depth as well (Fig. 9a,b).

The circulation in the WIM is affected by the entrance of the MW vein at the gateway between Cape St Vincent and the Gorringe Bank; furthermore, along its path around the WIM, the current sometimes becomes unstable and separates from the slope at different locations, generating recurrent anticyclonic structures (Meddies; Zenk and Armi 1990).

As consequence of the spreading process of the MW vein, when the flow turns into the Tagus Basin, the resulting mean flow is observed to generate mean vorticity structures, two of them (anticyclonic and cyclonic) trapped on the slope, denoted by A1 and C2 in Fig. 9b and an anticyclonic mean structure offshore denoted by A2. The resulting mean circulation is rather complex in the Tagus basin and on its northern side, near the Estremadura promontory in progress in the poleward direction, giving rise to a partial detachment and an anticyclonic structure, denoted A3, which extends from the MW levels up to the surface (Fig. 9a).

Evidences in the literature of this conspicuous negative vorticity in this region are discussed by Daniault et al. (1994) and Mazé et al. (1997). On the other hand, a region of anticyclonic vorticity is frequently observed near 40°N in the SST field, separating the southern waters (warmer and saltier) that progress in the poleward direction from the northern waters (fresher and colder). Also, a detailed discussion of this anticyclonic region in the framework of the dynamics of the IPC is presented by Peliz et al. (2003, 2005).

On the northern side of anticyclone A3, a flow bifurcation is observed (Fig. 9b). Part of the flow veers cyclonically and becomes part of a northwestward flow that leaves the domain at 42°N, 12°W south of the

Galicia Bank; the other part of the flow reattaches to the slope in the poleward direction, along Cape Finisterre at 43°N. The vertical structure of this poleward flow at this latitude can be seen in Fig. 10a, consisting in a poleward flow, associated with a downward slope of the isopycnal field centered at about 10°W, and extending in the vertical direction from the levels of MW up to the surface, while offshore of 10°W a weak equatorward flow is dominant.

The 43°N section in the work of Mazé et al. (1997) shows similar circulation, with poleward tendency maximum at ~9.75°W and equatorward flow from 10.5 to 12°W, which is attributed in part to the recirculation around the Galicia Bank.

The circulation at 50 m (Fig. 9a) shows patterns similar to those at 1,000 m showing coupling between the MW and the surface layers as further discussed below.

(b) Summer circulation

The summer circulation at the MW levels (Fig. 9d) presents a similar general behavior to that of winter discussed above. The inflow in the Tagus Basin occurs closer to the slope than in January.

The anticyclonic structure centered at 40°N, 11°W exhibits a weaker signature than the one observed in winter, which means a weaker tendency to detach from the northern flank of the Estremadura Promontory and hence stronger slope-trapped flow at the levels of the MW.

One of the most striking features in our modeled mean circulation for summer is the existence of conspicuous poleward flow. This issue will be further discussed below. Concerning the surface layers circulation (Fig. 9c), a band of equatorward flow along the continental shelf/upper slope is observed associated with the upwelling front with particular notice of the velocities between Cape Ortegal and Cape Finisterre. This flow is clearly visible in the vertical section at 43°N showing the structure of the upwelling front and an alongshore jet penetrating to a depth of about 400 m surrounded offshore by the poleward flow centered at about 10°W and again equatorward weak flow offshore in a similar way to the winter situation (Fig. 10a)

(c) Meridional transport

In order to get some insight about the seasonal and interannual variability of the circulation, series of alongshore transport were computed across three zonal sections at latitudes 43, 40, and 37.5°N and integrated in the upper 1,500 m depth range.

Each zonal section is divided into three subsections (hereafter called boxes for simplicity): shelf/upper slope (from the coast to the 400 m isobath), lower slope, and offshore box. These boxes will hereafter be designated as onshore, central, and offshore boxes, respectively. The width of the boxes is defined individually for each latitude because the location of both the upper and lower slope circulation varies with latitude. The border of the onshore box was designed to accommodate the shelf/upper slope circulation and was therefore defined by setting the depth at the 400 m isobath. The separation between the central and the offshore boxes was specified by defining the central box as the area of prevailing poleward flow.

Thus, monthly means of meridional net transport, with positive (negative) values corresponding to poleward (equatorward) flow, are shown for 43°N (Fig. 11a–c), 40°N (Fig. 11e–g), and 37.5°N (Fig. 11i–k).

In the onshore boxes (Fig. 11c,g,k), the main feature observed is the equatorward flow associated with upwelling, which presents one main peak centered in July–August and occasionally one or several minor peaks during spring. In wintertime, a poleward flow associated with the inshore intrusion of the IPC is observed on the upper slope. The equatorward summer transport peak is typically 0.5 Sv, independent of the latitude, but the spring peak varies from less than 0.1 Sv to about 0.3 Sv. Although a clear seasonal cycle of the circulation is seen for both upwelling and poleward flow, there is also some interannual variability in the structure of the peaks associated with the upwelling equatorward transport, both in width and intensity. Regarding the seasonal cycle, some differences can be observed in the equatorward circulation at different latitudes. In the northern and central sections (43 and 40°N, respectively; Fig. 11c,g), the equatorward flow starts early in the year (February) and lingers on until October, whereas in southern Portugal (37.5°N; Fig. 11k) a weak and variable circulation is observed during springtime (February to May) and the clear signal of upwelling appears in June–July. Furthermore, poleward flow along the shelf/upper slope is observed every year for the 43 and 40°N sections, with typical values of 0.2–0.3 Sv, starting at the beginning of autumn and with peaks in December, occasionally with secondary peaks in January. The southern region does not show clear evidences of poleward flow on the upper slope/shelf.

With respect to the central (Fig. 11b,f,j) and offshore (Fig. 11a,e,i) boxes, the transport patterns are not as clearly defined as in the case of the onshore box. For the northern and central latitudes (43 and 40°N) in the central box (Fig. 11b,f), two peaks of poleward flow are observed throughout the year in almost all simulation years: the first one during summertime (July to September), presenting high transport values, from 3 to 10 Sv; the second peak with smaller amplitudes, 2–7 Sv, is observed from November to January. Both transport peaks show

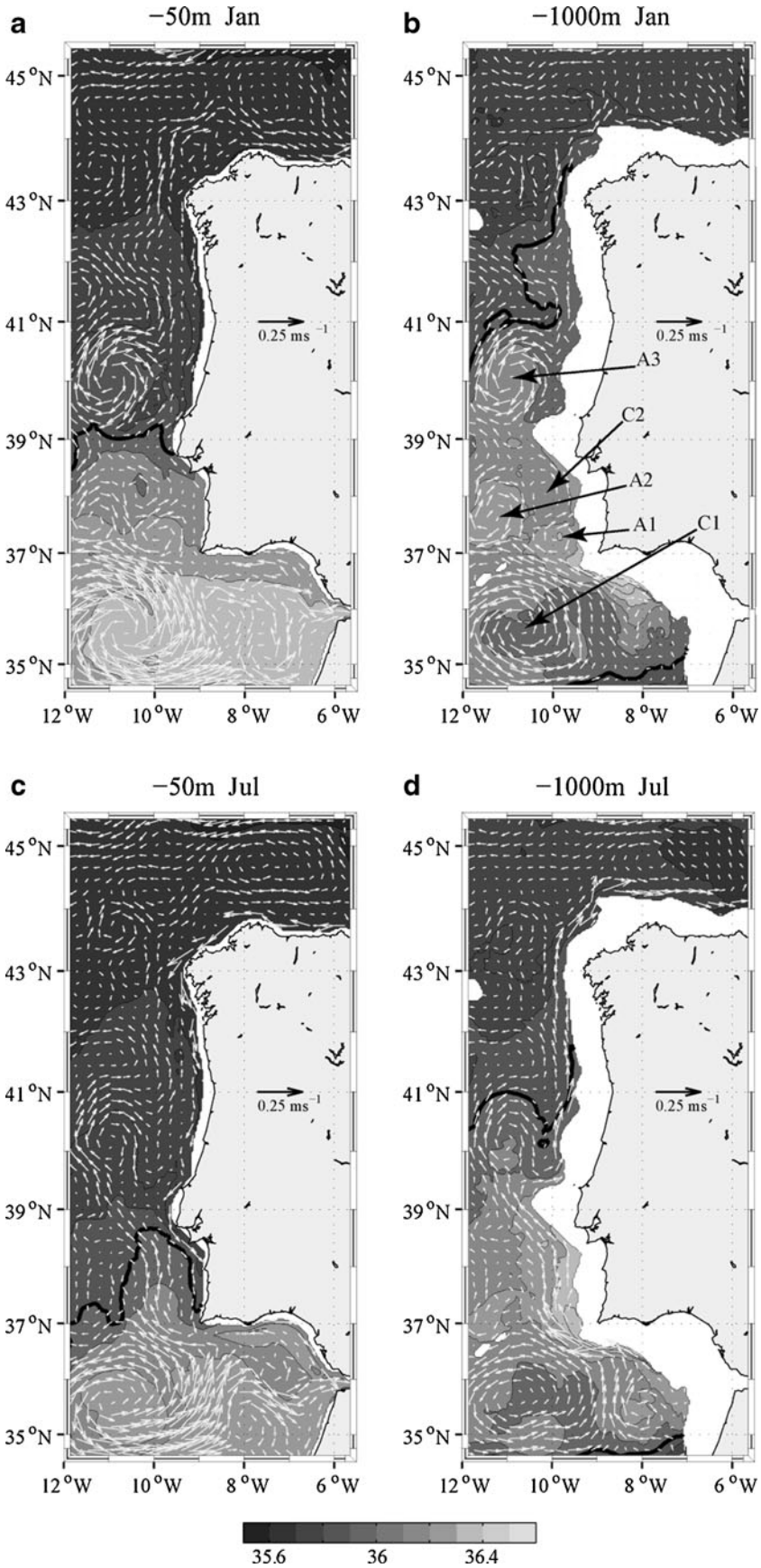

Fig. 9 Salinity and velocity fields for January (**a**,**b**) and July (**c**,**d**) at 50 m (**a**,**c**) and at 1,000 m (**b**,**d**). Isohalines are depicted every 0.2 (36 in *thick black contours*) and the vector scale is indicated on the map. For information regarding the *pointing arrows*, please refer to the text

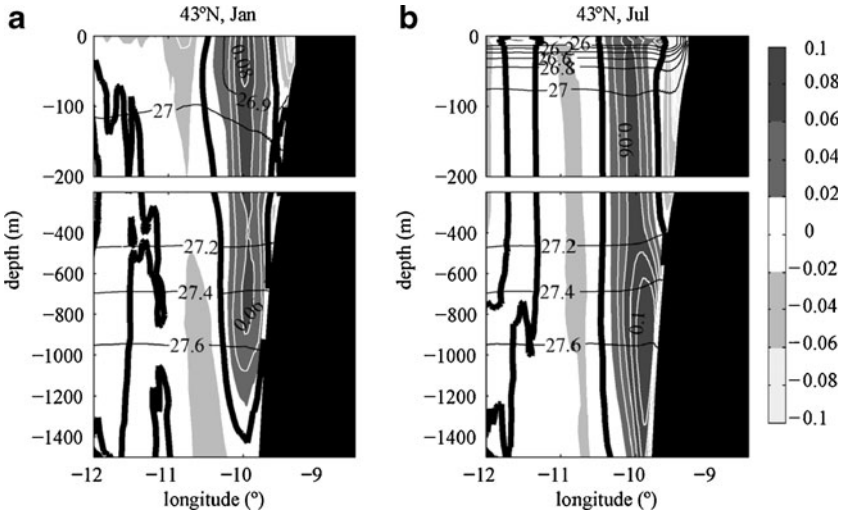

Fig. 10 Zonal sections, at 43°N, of 5-year means of potential density anomalies and meridional velocity for January (**a**) and July (**b**) down to 1,500 m deep. σ_θ is depicted every 0.2 kg m^{-3}. The *light shades of gray mark* negative values below −0.02 m s^{-1} and the *dark shades of gray* positive values above 0.02 m s^{-1}. The *thick contour* is zero and the first 200 m are enlarged

strong interannual variability. The first peak appears as an offshore poleward flow co-existing with the inshore summer upwelling peak (cf. Fig. 11b with c and Fig. 11f with g). This offshore shifting of poleward flow during upwelling season has also been reported in hydrographical cruises (Peliz et al. 2002; Torres and Barton 2007). The second peak is associated with the winter IPC. Conversely, every year, recurrent peaks of equatorward transport are observed during the late winter–spring months. The southern region in the central box (Fig. 11j) presents a complex pattern, although the tendency for poleward flow with multiple peaks during summer (shaded in Fig. 11j),

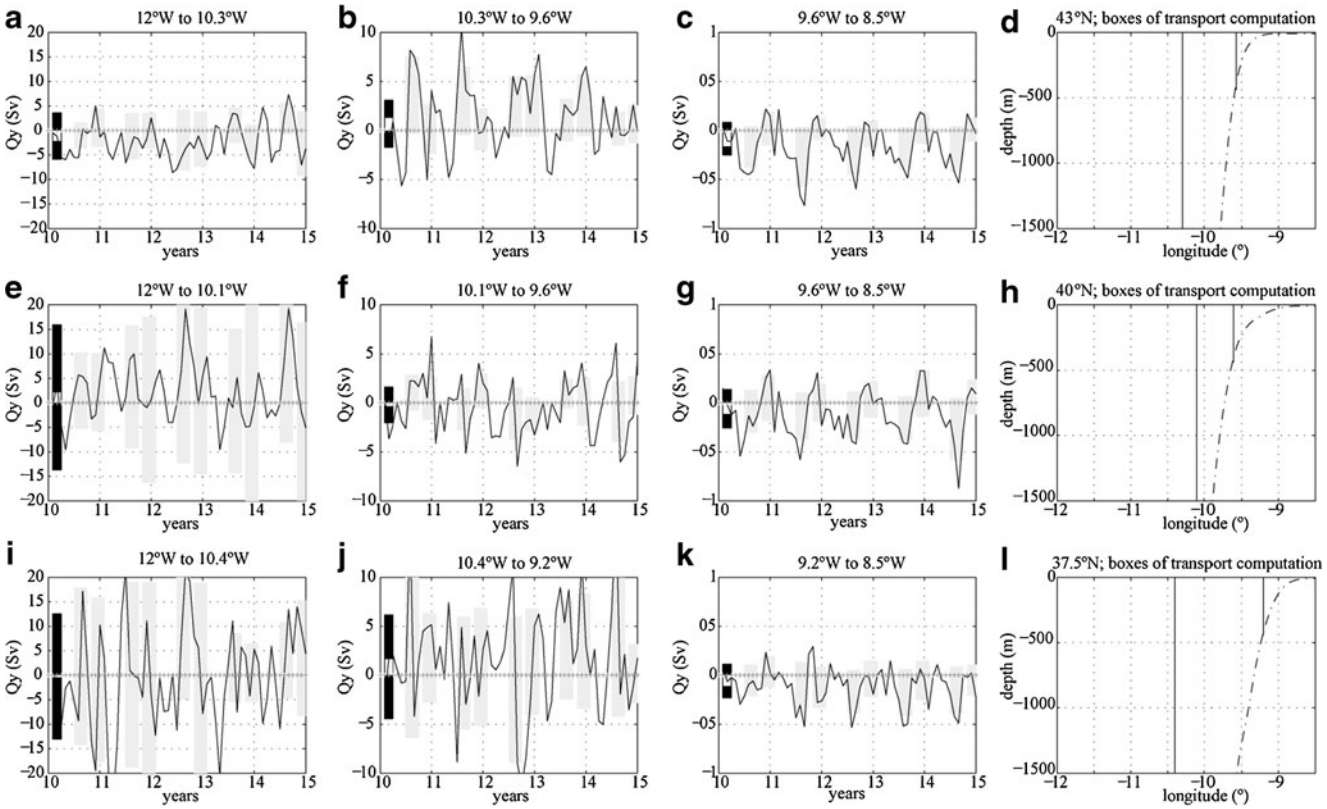

Fig. 11 Time series of meridional transport monthly means along: **a**–**d** 43°N, **e**–**h** 40°N, and **i**–**l** 37.5°N. Each column corresponds to a subsection represented in the rightmost column (**d**,**h**,**l**). From *left* to *right* **a**,**e**,**i** offshore; **b**,**f**,**j** lower slope and adjacent upper layers; **c**,**g**,**k** shelf/upper slope (down to 400 m). Seasonal averages (July, August, and September (JAS) and November, December, and January (NDJ)) are plotted in *shades of gray* for northward and southward transports. To the left of each plot, total northward and southward averages are in *black bars* and the net average is in *white bars*

late autumn, and January is still discernible. The tendency for equatorward flow observed during late winter and spring is only partially observed. Recall that this box is strongly influenced by the MW vein and the corresponding shedding of meddies, which makes it more difficult to interpret than the patterns described for the northern region.

The offshore region (Fig. 11a,e,i) is the widest of the three boxes and does not present a clear seasonal pattern as in the central and onshore boxes. The northern offshore box (Fig. 11a) is characterized by a tendency for equatorward flow, with typical values of less than 5 Sv, as previously discussed (Fig. 10a,b). This behavior is opposite to the one observed at the central box at the same latitude (Fig. 11b), which means that at 43°N the poleward flow is preferentially attached to the slope (central box), which Fig. 9b,d also shows. At 40°N (Fig. 11e), the offshore box is characterized by high values of transport in both directions resulting from the anticyclonic vorticity structure of the mean circulation (denoted A3 in Fig. 9b). However, the net overall transport in this box (Fig. 11e) is poleward during the summer months with strong interannual variability and, on the other hand, presents also peaks of poleward flow in February–March. This late winter poleward transport is delayed by 2–3 months relative to the peaks observed in the central box at 40°N (Fig. 11f), which can be interpreted as the westward IPC migration. On the other hand, the separation of the flow associated with A3 (Fig. 9b) occurring north of the Estremadura Promontory also explains the poleward tendency in this offshore box.

The southern (37.5°N) offshore region (Fig. 11i) is affected by a strong variability, consequence of the spreading of the MW vein, and its mesoscale features. However, like for the central offshore box (Fig. 11e), some features can be observed as peaks of poleward flow during summertime (shaded), and during November–January for most of the years, but also equatorward peaks between February and June every year.

3.4 Influence of the MW in the WIM circulation

One unique oceanographic feature in this region is the presence of the MW and its associated current patterns. Comparing the obtained circulation from a model configuration where the MW spreading through the Strait of Gibraltar was removed, with the base experiment, it is possible to get some insights into the influence of the MW spreading on the circulation of the region, which is closely linked to the density distribution at depth along WIM upper slope and to the dynamics of Atlantic surface and Central Waters and associated mesoscale activity.

The January and July mean circulation and salinity fields at 50 and 1,000 m in depth are displayed in Fig. 12, like for Fig. 7. Zonal sections of meridional velocity were also computed along latitudes 43°N for January and July, like for Fig. 10, and are shown in Fig. 13.

(a) Winter circulation

The 1,000 m current fields (Fig. 12b) present lower velocities in this no Mediterranean Water case (hereafter NMW) and there are less vorticity structures in the mean flow when compared to the base case. Poleward flow remains dominant at the surface and extends to ~1,000 m depth. The mean cyclonic recirculation cell signature to the south nearly disappears as it was associated to the MW outflow. In the Tagus Basin, there are no longer clear evidences of a region of vorticity structures, as it was in the base case (A1, A2, and C2 in Fig. 9b). North of the Estremadura Promontory, anticyclonic vorticity of the mean flow can still be observed but is much weaker than in the base case with velocities decreasing from 10 to 15 cm s^{-1} throughout the water column to 2–4 cm s^{-1} barely reaching the surface (Fig. 13a). Concerning the salinity field, weak horizontal gradients are observed at 1,000 m depth as expected due to the absence of MW.

Near the surface (Fig. 12a), the patterns of the mean velocity field are similar to those at 1,000 m depth with increased intensity. Poleward current is the prevailing pattern, with a continuous mean flow from the Gulf of Cadiz northwards, around Cape St Vincent and along the WIM. The surface poleward flow proceeds along northwestern Iberia with evidence of two branches: one narrow branch over the continental shelf (not visible in the base experiment) and another wider branch centered at about 10°W, both along the slope and extending eastwards into the Bay of Biscay with stronger intensity than in the base case. This double flow is also visible in the zonal sections (Fig. 13a).

A computation similar to the one depicted in Fig. 11 was carried out (not shown) and it further confirms the prevailing poleward flow in the continental shelf/upper slope (onshore boxes). Additionally, the mean annual balance is positive, that is, it surpasses the equatorward transport of upwelling.

Regarding the density distribution in depth near the upper slope (Figs. 10 and 13), there is a greater tendency for downward slope in the case of NMW than in the base experiment, which explains the strengthening of the poleward flow near the shelf. This increase in downward slope was also observed in other regions along the WIM (not shown). This stronger inshore poleward flow is also visible in the salinity field at 50 m depth (Fig. 12a), where the penetration of the 36 isohaline (marked in a thick contour) reaches farther north than in the base case, which presents nearly zonal isohalines.

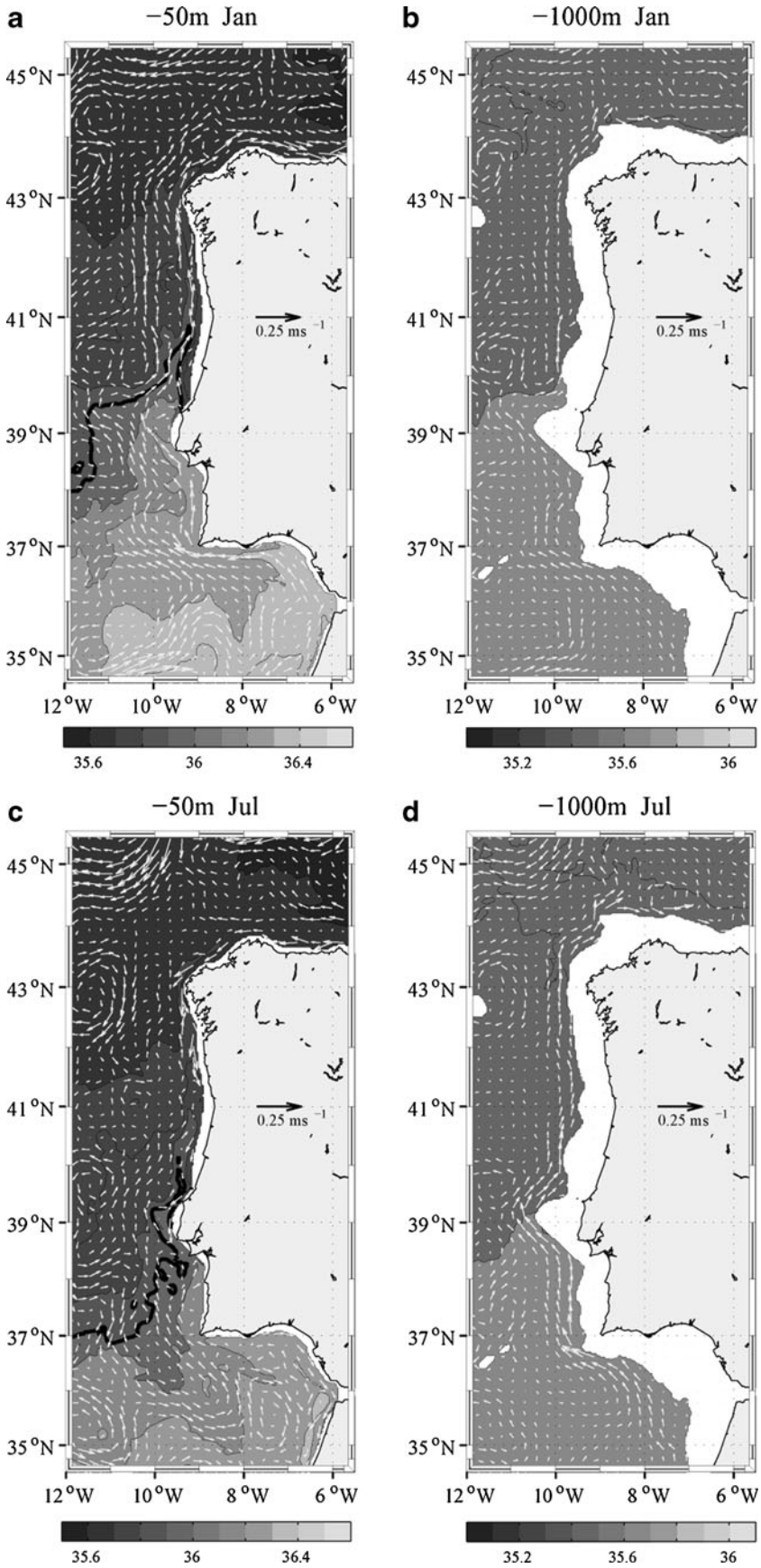

Fig. 12 Salinity and velocity fields for January (**a**,**b**) and July (**c**,**d**) at 50 m (**a**,**c**) and at 1,000 m (**b**,**d**) for the NMW run. Isohalines are depicted every 0.2 (36 in *thick black contours*) and the vector scale is indicated on the map

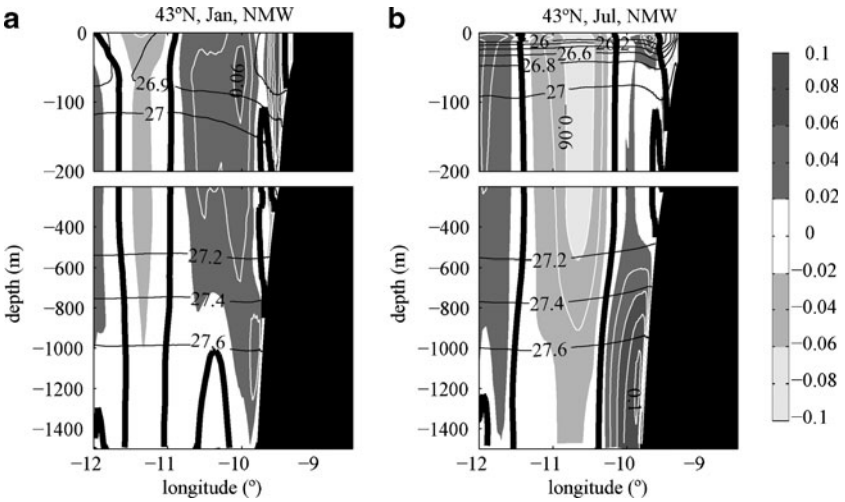

Fig. 13 Zonal sections, at 43°N, of 5-year means of potential density anomalies and meridional velocity for the NMW run for January (**a**) and July (**b**) down to 1,500 m deep. σ_θ is depicted every 0.2 kg m^{-3}. The *light shades of gray mark* negative values below −0.02 m s^{-1} and the *dark shades of gray* positive values above 0.02 m s^{-1}. The *thick contour* is zero and the first 200 m are enlarged

(b) Summer circulation

For July, the mean circulation patterns are similar to those of January for both 50 and 1,000 m depths (Fig. 12c,d), that is, there is a general weakening of the recirculation regions and a poleward flow tendency along the slope of WIM, as well as a farther northward penetration of the 36 isohaline. As for the meridional velocity zonal sections (Fig. 13b), we find that there is still the strong inshore poleward flow ramification observed in winter, which restricts upwelling to a thinner band on the continental shelf (less than 0.5° from the coast) and therefore also at depth, allowing the associated equatorward flow to spread only for the first 100–150 m.

In this way, the main effect of the absence of the MW vein on the mean circulation of WIM is the suppression or strong attenuation of a significant part of the recirculating flow associated with the mesoscale features characteristic of the MW spreading, such as shedding of meddies southwest of the Iberian Peninsula, whose signature in the mean flow are the structures depicted in Fig. 9b, β-plume cyclonic circulation in the Gulf of Cadiz, anticyclonic vorticity generation north of the Estremadura Promontory, and meandering along northwestern Iberia. As a consequence, the poleward flow seems to circulate more trapped to the slope between 10 and 9.5°W.

4 Discussion

The circulation of the Western Iberian Margin was studied by means of a high-resolution primitive equation numerical model. It was intended to model the seasonal cycle of the hydrographic fields and to study the associated circulation, resulting from the interaction of the three main phenomena: the upwelling, the Iberian Poleward Current system, and the Mediterranean water outflow.

The WIM ocean circulation is characterized by a complex oceanic system and it is influenced by large-scale phenomena like the eastward extension of the Azores Current, the structure of the meridional density gradient, or the less energetic Portugal offshore equatorward current. It is also influenced by small-scale localized phenomena like the exchange of waters through the Strait of Gibraltar, which spreads along the NE Atlantic. The river inflow also has influence on the circulation in the surface layers along the continental shelf and offshore.

The main focus of this study is to integrate the above mentioned phenomena into a numerical configuration that takes into account the large-scale phenomena and the local phenomena referred to above. The main objective is to study the mean hydrography and flow with special emphasis on the shelf/slope mean circulation and transports and its seasonal evolution. The connection between the intermediate circulation (at the MW levels) with the surface layers is explored and the prevalence of poleward slope flow along the summer.

(a) Circulation considerations

The forcing that we used lacks nonseasonal transient forcing and contains no interannual or synoptic meteorological scale variability. It was intended to model the hydrographic fields and to reach a realistic circulation as a result of the adjustment of the hydrographic fields. Concerning this resulting circulation, many of the modeled features have their correspondence in the available observations. The main pattern of the circulation consists in a poleward flow along the slope during winter, which lingers on in summer. In addition to the classic ideas related in the introduction, Torres and Barton (2006) described a complementary view of the initial development of the flow along northern WIP; they estimated a mean transport of 2 Sv from the surface down to 500 m and postulated that the poleward flow could

penetrate down to the levels of MW. The authors hypothesize that a poleward flow at the MW levels would arise from different dynamical reasons, but can form a continuous flow inducing topographic guidance of the surface flow. This behavior is well reproduced by the model results, suggesting that the poleward flow extends down to the levels of the MW (Fig. 12a–b).

The winter flow patterns obtained by the SD configuration resemble the typical description of poleward flow in the literature. The model results, as seen by the analyzed boxes (Fig. 11), also suggest interannual variability associated with the intrinsic variability and hence not resulting from external forcing.

However, this resulting interannual variability does not explain episodes of strong alongshore current observed in particular years only (January 1990, 1996, and 1998 as reported in Garcia-Soto et al. (2002) and Peliz et al. (2005)). This means that factors other than climatological forcing or large-scale forcing, both imposed seasonally but with no interannual variability, may explain the variability and the years of extreme poleward flow, not described within our simulations.

When considering the mean fields of hydrographic properties and alongshore velocity fields for several years, we obtain a picture of a poleward flow extending from the surface down to the levels of the MW, centered at about 10°W, with weak vertical shear and typical velocities of 6–10 cm s^{-1} for winter and summer, although with some weakening at the surface in this season (Fig. 10). This coupling between the MW and the Central Water layers was already suggested by Mazé et al. (1997). Moreover, observations of Huthnance et al. (2002) report maximum poleward flow at moorings near 42°N, 9.5°W in September–October for all depths, a secondary peak in December–January for the uppermost currentmeter, and a maximum of equatorward flow in February–April. These features resemble the transport patterns in the central box for section 43°N (Fig. 11b). Likewise, persistent poleward flow at about 250 m depth at a location near 42.3°N, 10.2°W is reported by Peliz et al. (2005) based on datasets of the Instituto Español de Oceanografía (Alonso et al. 1995), where the intensity of the poleward current was about 10 cm s^{-1} and no correlation between winds and currents was found at this mooring. This tendency for poleward flow at this longitude is comparable to the mean values presented in Fig. 10.

Concerning the issue related to the presence of poleward flow during the upwelling season, Peliz et al. (2002) presented evidences of such behavior for central Portugal. Torres and Barton (2007) studied the Galician shelf/slope based on hydrography and ADCP measurements and also showed the coexistence of offshore poleward flow during June 1997 at the start of the upwelling season. The model results suggest that poleward flow is present along the slope and coexist with the upwelling-associated flow along the shelf/upper slope. This is visible not only in the mean alongshore velocities but also in the transport associated with the central (slope) box (Fig. 11).

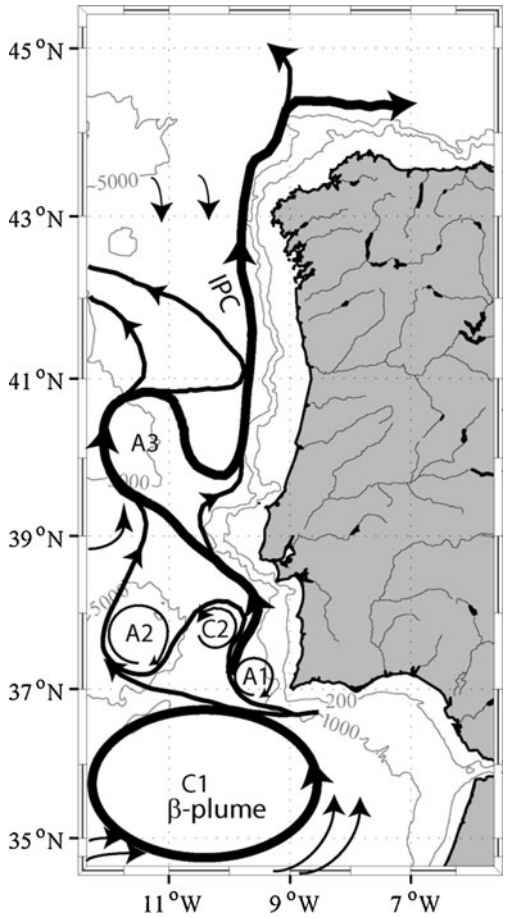

Fig. 14 Schematic representation of the mean circulation at 1,000 m as obtained from the present numerical modeling study showing the principal paths of the obtained circulation structures and the recirculation vorticity

(b) The influence of the MW flow on WIM

Concerning the experiment without explicit Mediterranean Water exchange at the Strait of Gibraltar, the resulting circulation consists in a general tendency for poleward currents in way similar to the SD experiment, which flows mainly trapped on the slope. The tendency for poleward flow regardless of the presence or absence of Mediterranean Water seems to be a robust result. However, the MW vein and its mesoscale features have strong influence on the poleward flow paths along the WIM, namely the enhancement of the separation north of Cape St Vincent, the promotion of strong anticyclonic recirculation north of the Estremadura Promontory, and

the separation at 41–42°N. The enhancement of the slope-trapped poleward flow is a noteworthy result given that one would expect the reverse by switching off the MW flow. There are a few possible reasons for this effect in the absence of MW spreading: (1) the absence of the associated positive thermohaline anomaly of the MW at mid-depths forces the density distribution at depth to re-arrange, so that the geostrophic adjustment at the slope, seen as a downward inflection of isopycnals, takes place at upper levels, as referred to above. As discussed in Huthnance (1984), geostrophic adjustment at western coasts produces the so-called Eastern Boundary Currents, which flow usually in subsurface in a direction opposite to that of the prevailing winds; (2) the almost disappearance of the cyclonic recirculation in the Gulf of Cadiz, the absence of detached anticyclonic structures throughout the WIM (meddies), and the absence of instabilities (meanders) associated with the absence of the MW vein, may allow a stronger slope-trapped poleward flow that would otherwise spread offshore, and at once a more stable flow along the WIM as it is observed in SD domain under NMW experiment. Consequently, lower levels of EKE were observed in the case of NMW (not shown); (3) several authors (e.g., Jia 2000; Kida et al. 2008; Volkov and Fu 2010) have hypothesized that there is a connection between the MW outflow in the Gulf of Cadiz and the recirculation of the Azores Current southwest of the Iberian Peninsula and even the very existence of that current. Therefore, the removal of the MW flow into the Atlantic may have implications at a larger spatial scale, which would then produce changes on the structure and intensity of the poleward flow. However, we cannot draw conclusions on this matter since our target domain (SD) does not enclose the Azores Current region.

The results suggest that in order to be able to realistically model the WIM circulation, a good representation of the MW spreading should be achieved including its associated mesoscale features that control the low-frequency circulation.

5 Conclusions

A numerical configuration was setup to resolve the ocean circulation at the Western Iberian Margin, based on climatological forcing, in order to study the resulting dynamical features of the surface layers down to the Mediterranean Water levels.

As a first step, the hydrographic fields resulting from the equilibrium solution were analyzed and compared to climatological values and we obtained reasonable results that allow exploring the associated circulation and studying of the mean seasonal velocity fields and associated transports.

The resulting circulation presents a tendency for poleward flow along the slope of the WIM but also evidences of equatorward flow mostly in spring. Also, as expected, wind-forced upwelling-driven equatorward flow is observed along the continental shelf in summer, in coexistence with poleward flow offshore. The main paths of poleward flow appear to be linked to the MW vein along the WIM.

A schematic view of the annual circulation at 1,000 m (which extends its main features up to the surface layers), showing the main paths of the mean circulation, is proposed in Fig. 14.

The MW vein enters through the Cape St Vincent–Gorringe Bank gateway and flows in the northwestward direction, separating from the southwestern slope of the Iberian Peninsula (near cape St Vincent) through an anticyclonic mean vorticity region (A1). Part of the flow continues poleward along the slope and part recirculates southward through a cyclonic mean vorticity region (C2) and continues poleward offshore due to the presence of another anticyclonic structure (A2). Both poleward branches, at the slope and offshore, give rise to the A3 anticyclonic region north of the Estremadura Promontory, although there is still flow along the slope, getting around the promontory. On the northern flank of this mean vorticity region, results suggest a new separation: part of the flow returns toward the coast and continues as the slope poleward flow, which is linked to the so-called IPC; the other part circulates poleward in another offshore branch between 11 and 12°W. The slope poleward flow seems to separate south of 42°N and joins the offshore branch, exiting afterwards the domain south of the Galicia Bank. The slope branch continues to flow northward along Cape Finisterre, with evidences of a separation at the northwestern tip of the Iberian Peninsula. Observational evidences for many of the features of this scheme can be found in the literature, as discussed above.

Acknowledgments The Fundação para a Ciência e Tecnologia (FCT) provided a PhD grant to ACP (SFRH/BD/47500/2008). This work is part of the "ISCAD—Inner shelf circulation and dispersion patterns: interactions with estuarine systems", PTDC/MAR/65760/2006 research project, also funded by the FCT under the European Regional Development Fund. This paper is also a contribution to CAIBEX project (CTM2007-66408-C02) (Spanish Ministry of Education and Science) and to RAIA project (0313_RAIA_1_E) funded by POCTEP and FEDER that supported NC grant.

References

Alonso J, de Castillejo FF, Diaz del Rio G, Marcote D, Casas G (1995) Preliminary results of current measurements in the North West of the Iberian Peninsula, MORENA Sci. and Tech. Rep. no 15, Instituto Espanol de Oceanografia C.O., La Coruna, Spain

Álvarez-Salgado XA, Figueiras FG, Pérez FF, Groom S, Nogueira E, Borges AV, Chou L, Castro CG, Moncoiffé G, Ríos AF, Miller AEJ,

Frankignoulle M, Savidge G, Wollast R (2003) The Portugal coastal counter current off NW Spain: new insights on its biogeochemical variability. Prog Oceanogr 56(2):281–321. doi:10.1016/S0079-6611(03)00007-7

Amante C, Eakins BW (2009) ETOPO1 1 Arc-minute global relief model: procedures, data sources and analysis. NOAA Tech. Memorandum NESDIS NGDC-24, 19 pp

Ambar I, Howe MR (1979) Observations of the Mediterranean outflow I—mixing in the Mediterranean outflow. Deep-Sea Res A 26(5): 535–554

Antonov JI, Seidov D, Boyer TP, Locarnini RA, Mishonov AV, Garcia HE, Baranova OK, Zweng MM, Johnson DR (2010) World Ocean Atlas 2009, volume 2: salinity. In: Levitus S (ed) NOAA Atlas NESDIS 69. U.S. Government Printing Office, Washington, 184 pp

Barja FJR, Lestegás FR (1992) Os Ríos Galegos–Morfoloxía e Réxime. Consello da Cultura Galega, Ponencia de Patrimonio Natural, Santiago de Compostela

Batteen ML, Martinez JR, Bryan DW, Buch EJ (2000) A modeling study of the coastal eastern boundary current system off Iberia and Morocco. J Geophys Res Oceans 105(C6):14173–14195

Batteen ML, Martinho AS, Miller HA, McClean JL (2007) A process-oriented modelling study of the coastal Canary and Iberian current system. Ocean Model 18:1–36

Bower AS, Armi L, Ambar I (1995) Direct evidence of meddy formation off the southwestern coast of Portugal. Deep-Sea Res I 42(9):1621–1630

Coelho HS, Neves RJJ, White M, Leitão PC, Santos AJ (2002) A model for ocean circulation on the Iberian coast. J Mar Syst 32(1–3):153–179. doi:10.1016/S0924-7963(02)00032-5

da Silva AM, Young CC, Levitus S (1994) Atlas of surface marine data 1994. NOAA Atlas NESDIS 10. U.S. Department of Commerce, NOAA, NESDIS

Daniault N, Mazé JP, Arhan M (1994) Circulation and mixing of Mediterranean water west of the Iberian Peninsula. Deep-Sea Res I 41(11–12):1685–1714. doi:10.1016/0967-0637(94)90068-X

Fiúza AFG (1984) Hidrologia e dinâmica das águas costeiras de Portugal, PhD thesis, University of Lisbon, 294 pp

Friocourt Y, Levier B, Speich S, Blanke B, Drijfhout S (2007) A regional numerical ocean model of the circulation in the Bay of Biscay. J Geophys Res Oceans 112, C09008. doi:10.1029/2006JC003935

Frouin R, Fiúza AFG, Ambar I, Boyd TJ (1990) Observations of a poleward surface current off the coasts of Portugal and Spain during winter. J Geophys Res Oceans 95(C1):679–691. doi:10.1029/JC095iC01p00679

García-Lafuente J, Sánchez Garrido JC, Díaz del Río G, Criado Aldeanueva F, Marcote D, Sánchez Román A (2008) Low-frequency variability of the Mediterranean undercurrent off Galicia, northwestern Iberian Peninsula. J Mar Syst 74(1–2):351–363. doi:10.1016/j.jmarsys.2008.02.007

Garcia-Soto C, Pingree RD, Valdés L (2002) Navidad development in the southern Bay of Biscay: climate change and swoddy structure from remote sensing and in situ measurements. J Geophys Res Oceans. doi:10.1029/2001JC001012

Haidvogel DB, Beckmann A (1999) Numerical ocean circulation modeling. Series on Environ Sci and Management, vol.2. Imperial College Press: London

Haynes R, Barton ED (1990) A poleward flow along the Atlantic coast of the Iberian Peninsula. J Geophys Res Oceans 95(C7):11425–11441. doi:10.1029/JC095iC07p11425

Huthnance JM (1984) Slope currents and "JEBAR". J Phys Oceanogr 14: 795–810

Huthnance JM, Van Aken HM, White M, Barton ED, Le Cann B, Ferreira Coelho E, Alvarez Fanjul E, Miller P, Vitorino J (2002) Ocean margin exchange—water flux estimates. J Mar Syst 32:107–137

Iorga MC, Lozier MS (1999) Signatures of the Mediterranean outflow from a North Atlantic climatology 1. Salinity and density fields. J Geophys Res Oceans 104(C11):25985–26009. doi:10.1029/1999JC900115

Jia Y (2000) Formation of an Azores Current due to Mediterranean overflow in a modeling study of the North Atlantic. J Phys Oceanogr 30:2342–2358. doi:10.1175/1520-0485(2000)030<2342:FOAACD>2.0.CO;2

Kida S, Price JF, Yang J (2008) The upper-oceanic response to overflows: a mechanism for the Azores Current. J Phys Oceanogr 38:880–895. doi:10.1175/2007JPO3750.1

Lamas L, Peliz Á, Ambar I, Barbosa Aguiar A, Maximenko N, Teles-Machado A (2010) Evidence of time-mean cyclonic cell southwest of Iberian Peninsula: the Mediterranean outflow-driven β-plume? Geophys Res Lett 37, L12606. doi:10.1029/2010GL043339

Large WG, McWilliams JC, Doney SC (1994) Oceanic vertical mixing: a review and a model with a nonlocal boundary-layer parameterization. Rev Geophys 32(4):363–403. doi:10.1029/94RG01872

Locarnini RA, Mishonov AV, Antonov JI, Boyer TP, Garcia HE, Baranova OK, Zweng MM, Johnson DR (2010) World Ocean Atlas 2009, volume 1: temperature. In: Levitus S (ed) NOAA Atlas NESDIS 68. U.S. Government Printing Office, Washington, 184 pp

Marchesiello P, McWilliams JC, Shchepetkin A (2001) Open boundary conditions for long-term integration of regional oceanic models. Ocean Model 3(1–2):1–20. doi:10.1016/S1463-5003(00)00013-5

Marchesiello P, Debreu L, Couvelard X (2009) Spurious diapycnal mixing in terrain-following coordinate models: the problem and a solution. Ocean Model 26(3–4):156–169. doi:10.1016/j.ocemod.2008.09.004

Mateus M, Riflet G, Chambel P, Fernandes L, Fernandes R, Juliano M, Campuzano F, de Pablo H, Neves R (2012) An operational model for the West Iberian coast: products and services. Ocean Sci 8:713–732

Mazé JP, Arhan M, Mercier H (1997) Volume budget of the eastern boundary layer off the Iberian Peninsula. Deep-Sea Res I 44(9–10):1543–1574. doi:10.1016/S0967-0637(97)00038-1

Neshyba S (1986) Poleward flows along eastern ocean boundaries. Springer: New York. ISBN 0387971750. p 374

Otero P, Ruiz-Villarreal M, Peliz A (2008) Variability of river plumes off Northwest Iberia in response to wind events. J Mar Syst 72(1–4): 238–255. doi:10.1016/j.jmarsys.2007.05.016

Paillet J, Arhan M, McCartney MS (1998) Spreading of Labrador Sea Water in the eastern North Atlantic. J Geophys Res Oceans 103(C5): 10223–10239. doi:10.1029/98JC00262

Peliz A, Rosa TL, Santos AMP, Pissarra JL (2002) Fronts, jets, and counter-flows in the Western Iberian upwelling system. J Mar Syst 35:61–77. doi:10.1016/S0924-7963(02)00076-3

Peliz A, Dubert J, Haidvogel DB, Le Cann B (2003) Generation and unstable evolution of a density-driven Eastern Poleward Current: the Iberian Poleward Current. J Geophys Res Oceans 108(C8):3268. doi:10.1029/2002JC001443

Peliz A, Dubert J, Santos AMP, Oliveira PB, Le Cann B (2005) Winter upper ocean circulation in the Western Iberian Basin—fronts, eddies and poleward flows: an overview. Deep-Sea Res I 52(4):621–646. doi:10.1016/j.dsr.2004.11.005

Peliz A, Dubert J, Marchesiello P, Teles-Machado A (2007) Surface circulation in the Gulf of Cadiz: model and mean flow structure. J Geophys Res Oceans. doi:10.1029/2007JC004159

Peliz A, Teles-Machado A, Marchesiello P, Dubert J, Garcia Lafuente J (2009) Filament generation off the strait of Gibraltar in response to gap winds. Dyn Ocean Atmos 46:36–45, doi: j.dynatmoce.2008.08.002

Penven P, Marchesiello P, Debreu L, Lefevre J (2008) Software tools for pre- and post-processing of oceanic regional simulations. Environ Model Softw 23(5):660–662. doi:10.1016/j.envsoft.2007.07.004

Pingree RD, Le Cann B (1990) Structure, strength and seasonality of the slope currents in the Bay of Biscay region. J Mar Biol Assoc U K 70: 857–885. doi:10.1017/S0025315400059117

Relvas P, Barton ED, Dubert J, Oliveira PB, Peliz A, da Silva JCB, Santos AMP (2007) Physical oceanography of the western Iberia ecosystem: latest views and challenges. Prog Oceanogr 74(2–3):149–173. doi:10.1016/j.pocean.2007.04.021

Reynaud T, Legrand P, Mercier H, Barnier B (1998) A new analysis of hydrographic data in the Atlantic and its application to an inverse modeling study. Inst WOCE Newsl 32:29–31

Richardson PL, Bower AS, Zenk W (2000) A census of Meddies tracked by floats. Prog Oceanogr 45(2):209–250

Ríos AF, Pérez FF, Fraga F (1992) Water masses in the upper and middle North Atlantic Ocean east of the Azores. Deep-Sea Res I 39(3–4): 645–658. doi:10.1016/0198-0149(92)90093-9

Røed LP, Shi XB (1999) A numerical study of the dynamics and energetics of cool filaments, jets and eddies of the Iberian Peninsula. J Geophys Res Oceans 104(C12):29817–29841. doi:10.1029/1999JC900175

Saunders PM (1982) Circulation in the eastern North Atlantic. J Mar Res 40:641–657

Serra N, Ambar I, Boutov D (2010) Surface expression of Mediterranean Water dipoles and their contribution to the shelf/slope–open ocean exchange. Ocean Sci 6:191–209

Shchepetkin AF, McWilliams JC (2003) A method for computing horizontal pressure-gradient force in an oceanic model with a nonaligned vertical coordinate. J Geophys Res Oceans 108(C3):3090. doi:10.1029/2001JC001047

Shchepetkin AF, McWilliams JC (2005) The regional oceanic modeling system (ROMS): a split-explicit, free-surface, topography-following-coordinate oceanic model. Ocean Model 9(4):347–404. doi:10.1016/j.ocemod.2004.08.002

Sibuet J-C, Monti S, Loubrieu B, Mazé J-P, Srivastava S (2004) Carte bathymétrique de l'Atlantique nord-est et du golfe de Gascogne: implications cinématiques. Bull Soc Geol Fr 175(5): 429–442

Stevens I, Hamann M, Johnson JA, Fiúza AFG (2000) Comparisons between a fine resolution model and observations in the Iberian shelf–slope region. J Mar Syst 26(1):53–74. doi:10.1016/S0924-7963(00)00038-5

Torres R, Barton ED (2006) Onset and development of the Iberian poleward flow along the Galician coast. Cont Shelf Res 26(10): 1134–1153. doi:10.1016/j.csr.2006.03.009

Torres R, Barton ED (2007) Onset of the Iberian upwelling along the Galician coast. Cont Shelf Res 27(13):1759–1778. doi:10.1016/j.csr.2007.02.005

Torres R, Barton ED, Miller P, Fanjul E (2003) Spatial patterns of wind and sea surface temperature in the Galician upwelling region. J Geophys Res Oceans 108(C4):3130. doi:10.1029/2002JC001361

Troupin C, Machín F, Ouberdous M, Sirjacobs D, Barth A, Beckers J-M (2010) High-resolution climatology of the northeast Atlantic using Data-Interpolating Variational Analysis (Diva). J Geophys Res Oceans 115, C08005. doi:10.1029/2009JC005512

Veitch J, Penven P, Shillington F (2010) Modeling equilibrium dynamics of the Benguela Current system. J Phys Oceanogr 40:1942–1964. doi:10.1175/2010JPO4382.1

Volkov DL, Fu L-L (2010) On the reasons for the formation and variability of the Azores Current. J Phys Oceanogr 40:2197–2220

Zenk W, Armi L (1990) The complex spreading pattern of Mediterranean Water off the Portuguese continental slope. Deep-Sea Res I 37(12): 1805–1823. doi:10.1016/0198-0149(90)90079-B